








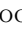






















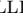
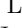

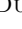


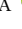


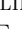



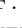


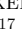













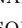


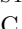
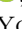






Inferring $M_{\text{BH}}-M_{\text{bulge}}$ Evolution from the Gravitational Wave Background

CAYENNE MATT ¹ KAYHAN GÜLTEKIN ¹ LUKE ZOLTAN KELLEY ² LAURA BLECHA ³ JOSEPH SIMON ^{4,*}
 GABRIELLA AGAZIE ⁵ AKASH ANUMARLAPUDI ⁶ ANNE M. ARCHIBALD ⁷ ZAVEN ARZOUMANIAN ⁸
 JEREMY G. BAIER ⁹ PAUL T. BAKER ¹⁰ BENCE BÉCSY ¹¹ ADAM BRAZIER ^{12,13} PAUL R. BROOK ¹¹
 SARAH BURKE-SPOLAOR ^{14,15,†} RAND BURNETTE⁹ ROBIN CASE⁹ J. ANDREW CASEY-CLYDE ¹⁶ MARIA CHARISI ¹⁷
 SHAMI CHATTERJEE ¹² TYLER COHEN ¹⁸ JAMES M. CORDES ¹² NEIL J. CORNISH ¹⁹
 FRONEFIELD CRAWFORD ²⁰ H. THANKFUL CROMARTIE ²¹ KATHRYN CROWTER ²² MEGAN E. DECESAR ^{23,‡}
 PAUL B. DEMOREST ²⁴ HELING DENG⁹ LANKESWAR DEY ^{14,15} TIMOTHY DOLCH ^{25,26}
 ELIZABETH C. FERRARA ^{27,28,29} WILLIAM FIORE ²² EMMANUEL FONSECA ^{14,15} GABRIEL E. FREEDMAN ⁵
 EMIKO C. GARDINER ² NATE GARVER-DANIELS ^{14,15} PETER A. GENTILE ^{14,15} KYLE A. GERSBACH¹⁷
 JOSEPH GLASER ^{14,15} DEBORAH C. GOOD ³⁰ C. J. HARRIS ¹ JEFFREY S. HAZBOUN ⁹ ROSS J. JENNINGS ^{14,15,§}
 AARON D. JOHNSON ^{5,31} MEGAN L. JONES ⁵ DAVID L. KAPLAN ⁵ MATTHEW KERR ³² JOEY S. KEY ³³
 NIMA LAAL ¹⁷ MICHAEL T. LAM ^{34,35,36} WILLIAM G. LAMB ¹⁷ BJORN LARSEN³⁷ T. JOSEPH W. LAZIO³⁸
 NATALIA LEWANDOWSKA ³⁹ TINGTING LIU ⁴⁰ DUNCAN R. LORIMER ^{14,15} JING LUO ^{41,¶} RYAN S. LYNCH ⁴²
 CHUNG-PEI MA ^{2,43} DUSTIN R. MADISON ⁴⁴ ALEXANDER MCEWEN ⁵ JAMES W. MCKEE ⁴⁵
 MAURA A. MCLAUGHLIN ^{14,15} NATASHA MCMANN ¹⁷ BRADLEY W. MEYERS ^{46,47} PATRICK M. MEYERS ³¹
 CHIARA M. F. MINGARELLI ³⁷ ANDREA MITRIDATE ⁴⁸ CHERRY NG ⁴⁹ DAVID J. NICE ⁵⁰
 STELLA KOCH OCKER ^{31,51} KEN D. OLUM ⁵² TIMOTHY T. PENNUCCI ⁵³ BENETGE B. P. PERERA ⁵⁴
 POLINA PETROV ¹⁷ NIHAN S. POL ⁵⁵ HENRI A. RADOVAN ⁵⁶ SCOTT M. RANSOM ⁵⁷ PAUL S. RAY ³²
 JOSEPH D. ROMANO ⁵⁵ JESSIE C. RUNNOE ¹⁷ ALEXANDER SAFFER ^{57,§} SHASHWAT C. SARDESAI ⁵
 ANN SCHMIEDEKAMP ⁵⁸ CARL SCHMIEDEKAMP ⁵⁸ KAI SCHMITZ ⁵⁹ BRENT J. SHAPIRO-ALBERT ^{14,15,60}
 XAVIER SIEMENS ^{9,5} SOPHIA V. SOSA FISCELLA ^{35,36} INGRID H. STAIRS ²² DANIEL R. STINEBRING ⁶¹
 KEVIN STOVALL ²⁴ ABHIMANYU SUSOBHANAN ⁶² JOSEPH K. SWIGGUM ^{50,§} JACOB TAYLOR⁹
 STEPHEN R. TAYLOR ¹⁷ MERCEDES S. THOMPSON²² JACOB E. TURNER ⁴² MICHELE VALLISNERI ^{38,31}
 RUTGER VAN HAASTEREN ⁶² SARAH J. VIGELAND ⁵ HALEY M. WAHL ^{14,15} KEVIN P. WILSON ^{14,15}
 CAITLIN A. WITT ⁶³ DAVID WRIGHT ⁹ AND OLIVIA YOUNG ^{35,36}

¹Department of Astronomy and Astrophysics, University of Michigan, Ann Arbor, MI 48109, USA

²Department of Astronomy, University of California, Berkeley, 501 Campbell Hall #3411, Berkeley, CA 94720, USA

³Physics Department, University of Florida, Gainesville, FL 32611, USA

⁴Department of Astrophysical and Planetary Sciences, University of Colorado, Boulder, CO 80309, USA

⁵Center for Gravitation, Cosmology and Astrophysics, Department of Physics, University of Wisconsin-Milwaukee, P.O. Box 413, Milwaukee, WI 53201, USA

⁶Department of Physics and Astronomy, University of North Carolina, Chapel Hill, NC 27599, USA

⁷Newcastle University, NE1 7RU, UK

⁸X-Ray Astrophysics Laboratory, NASA Goddard Space Flight Center, Code 662, Greenbelt, MD 20771, USA

⁹Department of Physics, Oregon State University, Corvallis, OR 97331, USA

¹⁰Department of Physics and Astronomy, Widener University, One University Place, Chester, PA 19013, USA

¹¹Institute for Gravitational Wave Astronomy and School of Physics and Astronomy, University of Birmingham, Edgbaston, Birmingham B15 2TT, UK

¹²Cornell Center for Astrophysics and Planetary Science and Department of Astronomy, Cornell University, Ithaca, NY 14853, USA

¹³Cornell Center for Advanced Computing, Cornell University, Ithaca, NY 14853, USA

¹⁴Department of Physics and Astronomy, West Virginia University, P.O. Box 6315, Morgantown, WV 26506, USA

¹⁵Center for Gravitational Waves and Cosmology, West Virginia University, Chestnut Ridge Research Building, Morgantown, WV 26505, USA

¹⁶Department of Physics, University of Connecticut, 196 Auditorium Road, U-3046, Storrs, CT 06269-3046, USA

¹⁷Department of Physics and Astronomy, Vanderbilt University, 2301 Vanderbilt Place, Nashville, TN 37235, USA

¹⁸Department of Physics, New Mexico Institute of Mining and Technology, 801 Leroy Place, Socorro, NM 87801, USA

¹⁹Department of Physics, Montana State University, Bozeman, MT 59717, USA

²⁰Department of Physics and Astronomy, Franklin & Marshall College, P.O. Box 3003, Lancaster, PA 17604, USA

²¹*National Research Council Research Associate, National Academy of Sciences, Washington, DC 20001, USA resident at Naval Research Laboratory, Washington, DC 20375, USA*

²²*Department of Physics and Astronomy, University of British Columbia, 6224 Agricultural Road, Vancouver, BC V6T 1Z1, Canada*

²³*Department of Physics and Astronomy, George Mason University, Fairfax, VA 22030, resident at the U.S. Naval Research Laboratory, Washington, DC 20375, USA*

²⁴*National Radio Astronomy Observatory, 1003 Lopezville Rd., Socorro, NM 87801, USA*

²⁵*Department of Physics, Hillsdale College, 33 E. College Street, Hillsdale, MI 49242, USA*

²⁶*Eureka Scientific, 2452 Delmer Street, Suite 100, Oakland, CA 94602-3017, USA*

²⁷*Department of Astronomy, University of Maryland, College Park, MD 20742, USA*

²⁸*Center for Research and Exploration in Space Science and Technology, NASA/GSFC, Greenbelt, MD 20771*

²⁹*NASA Goddard Space Flight Center, Greenbelt, MD 20771, USA*

³⁰*Department of Physics and Astronomy, University of Montana, 32 Campus Drive, Missoula, MT 59812*

³¹*Division of Physics, Mathematics, and Astronomy, California Institute of Technology, Pasadena, CA 91125, USA*

³²*Space Science Division, Naval Research Laboratory, Washington, DC 20375-5352, USA*

³³*University of Washington Bothell, 18115 Campus Way NE, Bothell, WA 98011, USA*

³⁴*SETI Institute, 339 N Bernardo Ave Suite 200, Mountain View, CA 94043, USA*

³⁵*School of Physics and Astronomy, Rochester Institute of Technology, Rochester, NY 14623, USA*

³⁶*Laboratory for Multiwavelength Astrophysics, Rochester Institute of Technology, Rochester, NY 14623, USA*

³⁷*Department of Physics, Yale University, New Haven, CT 06520, USA*

³⁸*Jet Propulsion Laboratory, California Institute of Technology, 4800 Oak Grove Drive, Pasadena, CA 91109, USA*

³⁹*Department of Physics and Astronomy, State University of New York at Oswego, Oswego, NY 13126, USA*

⁴⁰*Department of Physics and Astronomy, Georgia State University, 25 Park Place, Suite 605, Atlanta, GA 30303, USA*

⁴¹*Department of Astronomy & Astrophysics, University of Toronto, 50 Saint George Street, Toronto, ON M5S 3H4, Canada*

⁴²*Green Bank Observatory, P.O. Box 2, Green Bank, WV 24944, USA*

⁴³*Department of Physics, University of California, Berkeley, CA 94720, USA*

⁴⁴*Department of Physics, Occidental College, 1600 Campus Road, Los Angeles, CA 90041, USA*

⁴⁵*Department of Physics and Astronomy, Union College, Schenectady, NY 12308, USA*

⁴⁶*Australian SKA Regional Centre (AusSRC), Curtin University, Bentley, WA 6102, Australia*

⁴⁷*International Centre for Radio Astronomy Research (ICRAR), Curtin University, Bentley, WA 6102, Australia*

⁴⁸*Deutsches Elektronen-Synchrotron DESY, Notkestr. 85, 22607 Hamburg, Germany*

⁴⁹*Dunlap Institute for Astronomy and Astrophysics, University of Toronto, 50 St. George St., Toronto, ON M5S 3H4, Canada*

⁵⁰*Department of Physics, Lafayette College, Easton, PA 18042, USA*

⁵¹*The Observatories of the Carnegie Institution for Science, Pasadena, CA 91101, USA*

⁵²*Institute of Cosmology, Department of Physics and Astronomy, Tufts University, Medford, MA 02155, USA*

⁵³*Institute of Physics and Astronomy, Eötvös Loránd University, Pázmány P. s. 1/A, 1117 Budapest, Hungary*

⁵⁴*Arecibo Observatory, HC3 Box 53995, Arecibo, PR 00612, USA*

⁵⁵*Department of Physics, Texas Tech University, Box 41051, Lubbock, TX 79409, USA*

⁵⁶*Department of Physics, University of Puerto Rico, Mayagüez, PR 00681, USA*

⁵⁷*National Radio Astronomy Observatory, 520 Edgemont Road, Charlottesville, VA 22903, USA*

⁵⁸*Department of Physics, Penn State Abington, Abington, PA 19001, USA*

⁵⁹*Institute for Theoretical Physics, University of Münster, 48149 Münster, Germany*

⁶⁰*Giant Army, 915A 17th Ave, Seattle WA 98122*

⁶¹*Department of Physics and Astronomy, Oberlin College, Oberlin, OH 44074, USA*

⁶²*Max-Planck-Institut für Gravitationsphysik (Albert-Einstein-Institut), Callinstraße 38, D-30167 Hannover, Germany*

⁶³*Department of Physics, Wake Forest University, 1834 Wake Forest Road, Winston-Salem, NC 27109*

ABSTRACT

We test the impact of an evolving supermassive black hole (SMBH) mass scaling relation ($M_{\text{BH}}-M_{\text{bulge}}$) on the predictions for the gravitational wave background (GWB). The observed GWB amplitude is 2-3 times higher than predicted by astrophysically informed models which suggests the need to revise the assumptions in those models. We compare a semi-analytic model's ability to reproduce the observed GWB spectrum with a static versus evolving-amplitude $M_{\text{BH}}-M_{\text{bulge}}$ relation. We additionally consider the influence of the choice of galaxy stellar mass function on the modeled GWB spectra. Our models are able to reproduce the GWB amplitude with either a large number density of massive galaxies or a positively evolving $M_{\text{BH}}-M_{\text{bulge}}$ amplitude (i.e., the $M_{\text{BH}}/M_{\text{bulge}}$ ratio was higher in the past). If we assume that the $M_{\text{BH}}-M_{\text{bulge}}$ amplitude does not evolve, our models require a galaxy

stellar mass function that implies an undetected population of massive galaxies ($M_{\star} \geq 10^{11} M_{\odot}$ at $z > 1$). When the $M_{\text{BH}}-M_{\text{bulge}}$ amplitude is allowed to evolve, we can model the GWB spectrum with all fiducial values and an $M_{\text{BH}}-M_{\text{bulge}}$ amplitude that evolves as $\alpha(z) = \alpha_0(1+z)^{1.04 \pm 0.5}$.

1. INTRODUCTION

In mid-2023, four pulsar timing array (PTA) collaborations announced evidence for the gravitational wave background (GWB) (R. W. Hellings & G. S. Downs 1983; G. Agazie et al. 2023a; EPTA Collaboration et al. 2023; D. J. Reardon et al. 2023; H. Xu et al. 2023). In all four announcements, the strain amplitude of the signal was 2–3 times greater than expected. It is commonly thought that the source for this quadrupolar signal is dominated by supermassive black hole (SMBH) binaries (M. C. Begelman et al. 1980; M. Milosavljević & D. Merritt 2001; S. Burke-Spolaor et al. 2019). In this case, the GWB amplitude is most sensitive to the chirp mass of the binaries and is therefore expected to be dominated by the most massive binaries (E. S. Phinney 2001). Thus, to model the GWB, it is necessary to have a reliable way to characterize the mass distribution of the underlying SMBH binary population. To make meaningful astrophysical inferences from PTA data it is therefore important to have an accurate predictor for the black hole mass function (BHMF), especially for the most massive SMBHs.

In the local universe, it has been shown that there is a strong correlation between host galaxy bulge mass and central SMBH mass, making it possible to accurately predict SMBH masses in nearby galaxies. Direct, independent SMBH mass measurements are difficult outside the local universe, however, and so very few constraints exist for this relation for $z > 0$. High redshift SMBH mass measurements are hindered by telescope resolution limits meaning that masses must be inferred indirectly. Because of their extreme luminosity, AGN can be used to place useful constraints on SMBH masses at redshifts as high as $z \sim 10$ (J. Jeon et al. 2025; Á. Bogdán et al. 2024; R. Maiolino et al. 2024a; L. Napolitano et al. 2024). From the AGN luminosity function, one can infer the BHMF, but assumptions about, e.g., radiative efficiency and AGN fraction lead towards large uncertainties (X. Shen et al. 2020). Furthermore, these types of surveys are frequently magnitude limited and

are thus subject to observational biases (T. R. Lauer et al. 2007).

While AGN studies inform SMBH populations, modeling the GWB calls for a simpler BHMF framework. The observed correlation between galaxy bulge mass and SMBH mass is known as the $M_{\text{BH}}-M_{\text{bulge}}$ relation (J. Kormendy & L. C. Ho 2013; N. J. McConnell & C.-P. Ma 2013). To approximate SMBH number density at higher redshifts, one can convolve the local $M_{\text{BH}}-M_{\text{bulge}}$ relation with the galaxy stellar mass function (GSMF), which is well-observed for the redshifts where most of the GWB signal is expected to be produced ($0 < z < 2$ A. Sesana et al. 2004; G. Agazie et al. 2023b; J. Leja et al. 2020). This method assumes the $M_{\text{BH}}-M_{\text{bulge}}$ relation to be unchanging with time, an assumption with ambiguous observational support. G. Agazie et al. (2023b) derived physical quantities from fitting the NANOGrav 15-year PTA data and their results suggested that the data are best described with a number density of SMBHs, with $M_{\text{BH}} \gtrsim 10^9 M_{\odot}$, that is notably greater than predictions from current models (such as J. Kormendy & L. C. Ho 2013; N. J. McConnell & C.-P. Ma 2013). Since then, other studies have used a variety of techniques finding similar results (e.g., G. Sato-Polito et al. 2024; Y. Chen et al. 2024; E. R. Liepold & C.-P. Ma 2024). Additionally, there exist other scaling relations, such as the $M_{\text{BH}}-\sigma$ relation, which connects SMBH mass to galaxy velocity dispersion (L. Ferrarese & D. Merritt 2000; K. Gebhardt et al. 2000). It has been shown that the $M_{\text{BH}}-M_{\text{bulge}}$ and $M_{\text{BH}}-\sigma$ relations make different predictions for the BHMF at high redshift such that the predicted GWB is higher when using $M_{\text{BH}}-\sigma$ (C. Matt et al. 2023; J. Simon 2023). This difference in BHMF predictions may be due to evolution in one or both relations that is not accounted for. Via the three-way relationship between galaxy stellar mass, radius, and velocity dispersion (A. de Graaff et al. 2021), the $M_{\text{BH}}-\sigma$ relation naturally accounts for galaxy downsizing (A. van der Wel et al. 2014) and may therefore be a more fundamental probe of the SMBH's gravitational potential well than $M_{\text{BH}}-M_{\text{bulge}}$ (R. C. E. van den Bosch 2016; J. H. Cohn et al. 2025). This combination of findings suggests that methods of predicting SMBH number density are in need of revision.

It is unknown when the $z = 0$ $M_{\text{BH}}-M_{\text{bulge}}$ relation was first established or how accurate it is outside the local universe. The strong local correlation between SMBH mass and galaxy bulge mass suggests the growth

* NSF Astronomy and Astrophysics Postdoctoral Fellow

† Sloan Fellow

‡ Resident at the Naval Research Laboratory

§ NANOGrav Physics Frontiers Center Postdoctoral Fellow

¶ Deceased

of these objects is coupled (J. Kormendy & L. C. Ho 2013). If the $M_{\text{BH}}-M_{\text{bulge}}$ relation were to be unchanging with time, it would suggest a lockstep growth for galaxies and SMBHs. In other words, galaxy star formation matches the pace of SMBH accretion and / or the dominant growth mechanisms for both of these bodies are through major mergers or positive AGN/stellar feedback. It is unknown, however, whether SMBHs grow faster than their host galaxies, vice versa, or if they grow symbiotically over cosmic time. Whether a galaxy's SMBH is over- or undermassive relative to the $M_{\text{BH}}-M_{\text{bulge}}$ relation throughout time has implications for the interactions between feedback from AGN accretion and galactic star formation (M.-Y. Zhuang & L. C. Ho 2023; J. H. Cohn et al. 2025). Constraints on these growth pathways are necessary for determining SMBH number density and galaxy evolution outside the local universe.

Results from the *James Webb Space Telescope* (JWST) have found galaxies at high redshift ($z > 4$) with overmassive black holes entirely unpredicted by the local $M_{\text{BH}}-M_{\text{bulge}}$ relation (e.g., Y. Harikane et al. 2023; F. Pacucci et al. 2023; J. Matthee et al. 2024; I. Juodžbalis et al. 2025). These high-redshift black holes are unexpectedly high in both mass and number density, with candidates up to $z \sim 11$ (e.g. R. Maiolino et al. 2024b). Furthermore, there is an abundance of observational and simulation-based studies that have found evidence both for and against an evolution in the amplitude of the $M_{\text{BH}}-M_{\text{bulge}}$ relation (e.g., J. S. B. Wyithe & A. Loeb 2003; A. Cattaneo et al. 2005; C. Y. Peng et al. 2006; D. J. Croton 2006; P. F. Hopkins et al. 2009; K. Jahnke et al. 2009; R. Decarli et al. 2010; A. Merloni et al. 2010; B. Trakhtenbrot & H. Netzer 2010; V. N. Bennert et al. 2011; M. Cisternas et al. 2011; X. Ding et al. 2020; J. Li et al. 2021; Y. Zhang et al. 2023; F. Pacucci et al. 2023; B. A. Terrazas et al. 2024; M. Yue et al. 2024; Y. Chen et al. 2024; A. P. Cloonan et al. 2024; M. R. Sah & S. Mukherjee 2024; M. R. Sah et al. 2024; T. Shimizu et al. 2024; F. Pacucci & A. Loeb 2024; A. Hoshi et al. 2024; M. M. Kozhikkal et al. 2024; Y. Sun et al. 2025; T. S. Tanaka et al. 2025).

An $M_{\text{BH}}-M_{\text{bulge}}$ amplitude that changes with cosmic time would have a significant impact on GWB predictions and interpretations. For example, if SMBH growth generally outpaces galaxy growth at higher redshifts, the $z = 0$ $M_{\text{BH}}-M_{\text{bulge}}$ relation would therefore underestimate SMBH masses which would, in turn, lead to an underestimate of the GWB amplitude. Past studies have used electromagnetic (EM) observation, theory, and simulations to constrain potential evolution in the $M_{\text{BH}}-M_{\text{bulge}}$ relation, and now gravitational waves offer a new, independent, basis for testing.

If, instead, the $M_{\text{BH}}-M_{\text{bulge}}$ relation that is measured locally has not changed significantly since $z \sim 3$, a higher number density of massive galaxies in this redshift range could explain the high GWB amplitude. The galaxy stellar mass function (GSMF) is not observed to undergo significant evolution from $z = 1$ to $z = 0$ (e.g., J. Leja et al. 2020) though theory predicts otherwise (e.g., S. Tacchella et al. 2019). Recently E. R. Liepold & C.-P. Ma (2024) found that this lack of observed evolution may be an artifact of the survey design. They explain that, locally, the most massive galaxies are rare enough that most current integral-field spectroscopic surveys do not observe a large enough volume to catch them. This leads to an incomplete local sample for galaxies with masses $M_{\star} \geq 10^{11.5} M_{\odot}$. Using the MASSIVE survey (which has a $107'' \times 107''$ field of view, C.-P. Ma et al. 2014) E. R. Liepold & C.-P. Ma (2024) measured a new $z = 0$ GSMF based on this sample and found that the number density of these massive galaxies is significantly higher than other measurements (such as M. Bernardi et al. 2013; J. Moustakas et al. 2013; R. D'Souza et al. 2015; J. Leja et al. 2020). Their work suggests that predictions for the GWB may have previously been under counting the number of the most massive galaxies, and therefore SMBHs, which could lead to an underestimate of the GWB amplitude. This intriguing possibility warrants further testing.

In this paper we evaluate the possibility of an evolving $M_{\text{BH}}-M_{\text{bulge}}$ amplitude and test the impact of this evolution on the GWB spectrum. We additionally consider changes to the GSMF and explore the degeneracy between these two solutions. In section 2 we describe our model setup including our functional form of redshift evolution of the $M_{\text{BH}}-M_{\text{bulge}}$ relation. In section 3 we present the results of our models. We discuss the implications of our work in section 4, and a summary of our work and conclusions can be found in section 5.

2. METHODS

In this section we describe the general setup of our semi-analytic model and our choices for the $M_{\text{BH}}-M_{\text{bulge}}$ scaling relation and GSMF. We additionally provide details for the priors and assumptions for our different test cases in section 2.4.

2.1. Semi-Analytic Modeling

We use HOLODECK (details can be found in section 3 of G. Agazie et al. 2023b)¹ to synthesize populations of massive black holes. We start by convolving the galaxy stellar mass function from J. Leja et al. (2020) with the

¹ Also see <https://github.com/nanograv/holodeck>.

SMBH–galaxy mass scaling relation from (J. Kormendy & L. C. Ho 2013). The specifics of this implementation are detailed in sections 2.2 and 2.3. We then apply galaxy merger rates, and SMBH binary hardening models to solve for the number density of SMBH binaries emitting gravitational waves in frequencies detectable by PTAs, i.e., the GWB spectrum predicted from the input parameters. Previously, G. Agazie et al. (2023b) calculated galaxy merger rates from galaxy pair fractions and merger times following the prescription due to (S. Chen et al. 2019a). For this work, we instead use the galaxy merger rate prescription due to V. Rodriguez-Gomez et al. (2015). A detailed description and graphic of the HOLODECK workflow can be found in section 3 of G. Agazie et al. (2023b).

To determine our best-fit parameters for each model, we first sampled 20,000 times from a set of astrophysically-motivated prior distributions with a Latin hypercube. We generated and averaged over 100 realizations for each set of sampled parameters to account for the Poisson sampling in the GWB spectrum calculations. Our sample size is higher than was used in G. Agazie et al. (2023b), who used Gaussian process interpolation for their posterior parameter estimation. Because of our larger parameter space (up to 30 parameters versus their 6), it is not computationally feasible to follow their same methods (N. Laal et al. 2025). Instead, our finer sampling makes it so that we can compare each model to the spectrum without the need for Gaussian process interpolation between the models. We compare our models to the 15 year HD-correlated free-spectrum representation of the GWB (specifically, we use the “HD-w/MP+DP+CURN” case which is detailed further in G. Agazie et al. 2023a; W. G. Lamb et al. 2023). For each GWB frequency, we evaluate the goodness of fit for a given modeled spectrum by comparing the value of each model to the probability density distribution of the data to determine how well each model fits the data. This process produces results with the same fidelity as G. Agazie et al. (2023b) with a higher computational efficiency (see their Appendix C, also our figures in Appendix C).

2.2. The $M_{\text{BH}}-M_{\text{bulge}}$ relation

The local relation between SMBH and galaxy bulge mass can be described by a power-law relation (see, e.g., J. Kormendy & K. Gebhardt 2001; J. Kormendy & L. C. Ho 2013; N. J. McConnell & C.-P. Ma 2013). The value of the y -intercept (amplitude) of this relation, throughout time, encodes the extent to which SMBHs and galaxies grow at the same rate. A constant amplitude value means that growth is tightly coupled and

the coupling mechanisms are constant throughout cosmic time. In this work, we model a changing amplitude with a power-law evolution. We modified the existing $M_{\text{BH}}-M_{\text{bulge}}$ framework in HOLODECK to allow for this evolution by replacing the constant amplitude with one that is a function of redshift, $\alpha_0 \rightarrow \alpha(z)$. We parameterize it as

$$M_{\text{BH}} = \alpha(z) \left(\frac{M_{\text{bulge}}}{10^{11} M_{\odot}} \right)^{\beta_0} \quad (1)$$

with

$$\alpha(z) = \alpha_0(1+z)^{\alpha_z}, \quad (2)$$

where the $z = 0$ values can be determined from observation ($\log \alpha_0 = 8.69$; $\beta_0 = 1.17$; J. Kormendy & L. C. Ho 2013), and α_z can be positive or negative with $\alpha_z = 0$ indicating no evolution in the relation.

This power-law form of evolution is more rapid at lower redshifts, which means that the changes in the $M_{\text{BH}}-M_{\text{bulge}}$ relation are greatest in the redshift range most relevant to the GWB ($0 < z < 2$, A. Sesana et al. 2004; G. Agazie et al. 2023b). We tested several functional forms of this evolution and determined that other options either evolve too slowly in the relevant redshift range, or are not distinguishable from a power-law with the current data. Future studies with higher signal-to-noise PTA data may eventually be able to place constraints on different functional forms, but until then, the power-law form is sufficient for this analysis. Throughout this analysis, we use the J. Kormendy & L. C. Ho (2013) values for the local $M_{\text{BH}}-M_{\text{bulge}}$ relation; we briefly discuss the impact of using alternative fits in Appendix A.

2.3. The Galaxy Stellar Mass Function

G. Agazie et al. (2023b) used the single-Schechter (P. Schechter 1976) GSMF prescription due to S. Chen et al. (2019b). For this work, we predominantly use the GSMF due to J. Leja et al. (2020), which is defined as a double-Schechter function offering a more accurate description of the mass function of the total galaxy population (e.g., D. J. McLeod et al. 2021, and references therein). This GSMF is strongly supported by observational data and has an explicitly defined evolution making it possible to reliably calculate the GSMF at any specific redshift, even extrapolating outside the range of the data ($0.2 < z < 3$). J. Leja et al. (2020) find that the redshift evolution of the characteristic mass and each of the density normalization terms is best described by a Gaussian. Following their methods (see their equations 14 and B 1-4), we define the full functional form of the

GSMF to be

$$\Phi(M_*, z) = \ln(10) \exp \left[-\frac{M_*}{M_c(z)} \right] \times \left(\phi_{*,1}(z) \left(\frac{M_*}{M_c(z)} \right)^{\alpha_1+1} + \phi_{*,2}(z) \left(\frac{M_*}{M_c(z)} \right)^{\alpha_2+1} \right) \quad (3)$$

where

$$\log \phi_{*,i}(z) = \phi_{*,i,0} + \phi_{*,i,1}z + \phi_{*,i,2}z^2, \quad (4)$$

and

$$\log M_c(z) = M_{c,0} + M_{c,1}z + M_{c,2}z^2. \quad (5)$$

$M_c(z)$ is the characteristic mass, $\phi_{*,i}(z)$ is density normalization, and α_1 and α_2 are the upper and lower slopes of the power-law.

Recently, [E. R. Liepold & C.-P. Ma \(2024\)](#) developed a $z = 0$ GSMF which has a notably higher number density than that of [J. Leja et al. \(2020\)](#) for $M_* \gtrsim 10^{11.5} M_\odot$. They make an estimate of the GWB amplitude and conclude that, using their local GSMF and an implied redshift evolution informed by the fractional GWB contribution functions from [G. Agazie et al. \(2023b\)](#) (see their Figure 12). Using their GSMF they claim they can produce a GWB amplitude that is consistent with what is seen by PTAs. Motivated by their results, we also consider how changes to the GSMF could instead explain the discrepancy between the predicted and observed GWB amplitude. [E. R. Liepold & C.-P. Ma \(2024\)](#) do not provide an explicit evolutionary form for their GSMF and so we assume an evolution that is equivalent to their $z = 0$ GSMF and consistent with [J. Leja et al. \(2020\)](#) for $z \gtrsim 1$. Further details of this evolution and discussion of alternative models can be found in Appendix A.

2.4. The Models

We present 8 models, which are summarized in Table 1. There are four different parameter setups and for each setup we ran one version of the model using the non-evolving $M_{\text{BH}}-M_{\text{bulge}}$ relation, and one version with evolution. For the models that allow for evolution of the $M_{\text{BH}}-M_{\text{bulge}}$ amplitude, we used a uniform prior for the evolutionary parameter $-3 \leq \alpha_z \leq 3$.

The largest models include 29 parameters (30 with α_z). Of these parameters, the GSMFs make up 11 variables, five that describe the local GSMF and six that contain information about the GSMF evolution. To help understand the degeneracy between a changing GSMF versus $M_{\text{BH}}-M_{\text{bulge}}$ relation we consider three different cases of sampling the GSMF: one in which we sample all 11 variables (Le11ne and Le11ev), one in which we only

Model Name	GSMF Parameters	Evolving $M_{\text{BH}}-M_{\text{bulge}}$
Le11ne	11 sampled	No
Le11ev	11 sampled	Yes
Le03ne	3 sampled	No
Le03ev	3 sampled	Yes
Le00ne	0 sampled	No
Le00ev	0 sampled	Yes
LM11ne	11 sampled	No
LM11ev	11 sampled	Yes

Table 1. A summary of the parameter set up for the 8 models in this paper. The naming convention for our models is xxyyzz where xx gives the source for the GSMF (Le for [J. Leja et al. \(2020\)](#) and LM for [E. R. Liepold & C.-P. Ma \(2024\)](#)), yy dictates the number of GSMF parameters that were sampled (out of 11 possible) and zz indicates whether the $M_{\text{BH}}-M_{\text{bulge}}$ amplitude was evolving (ev) or not evolving (ne). All but two of the models use our fiducial GSMF from [J. Leja et al. \(2020\)](#). The remaining two of the models are based on an explicitly evolving form of the [E. R. Liepold & C.-P. Ma \(2024\)](#) GSMF which we define in section 2.3.

sample three local values (Le03ne and Le03ev), and one with all GSMF parameters fixed to their fiducial values (Le00ne Le00ev). The three GSMF values that are varied in Le03ne and Le03ev are $\log \phi_{*,1,0}$, $\log \phi_{*,2,0}$, and $\log M_{c,0}$. For all but 2 of our 8 models we use the Gaussian posteriors from [J. Leja et al. \(2020\)](#) as priors for our GSMF and we assume that these parameters are independent of each other. For the last two models, we use our explicitly evolving version of the [E. R. Liepold & C.-P. Ma \(2024\)](#) GSMF, which we described previously in section 2.3 and also in appendix section A.

Each model we present is given a short-hand name to indicate the important features. Each name is 6 total characters to convey three pieces of information: The first two characters indicate which version of the GSMF is being used where Le is [J. Leja et al. \(2020\)](#) and LM is [E. R. Liepold & C.-P. Ma \(2024\)](#). The middle two characters indicate how many of the GSMF parameters (out of 11) were sampled where the number of parameters fixed to their fiducial values is 11 minus that number. The final two characters indicate whether the $M_{\text{BH}}-M_{\text{bulge}}$ amplitude was allowed to evolve (ev) or not (ne). This information is summarized in Table 1.

Because the models with evolving $M_{\text{BH}}-M_{\text{bulge}}$ relations are a strict parametric super set of those without (i.e., the models are nested), we performed Savage-Dickey ratio tests to quantify the significance of the evolving model over the fixed model ([J. M. Dickey 1971](#); [E.-J. Wagenmakers et al. 2010](#)). For all our figures and

Model Name	α_z	% Positive	S-D Ratio
Le11ev	0.84 ± 0.79	87.2	1.3
Le03ev	1.02 ± 0.48	99.3	24.6
Le00ev	1.05 ± 0.55	96.8	5.2
LM11ev	0.86 ± 0.76	88.7	1.5

Table 2. The values of α_z and significance of each of our evolving models. Each quoted value for α_z is the median of the posterior and the associated error represents the 68% confidence interval. We report the percentage of the posterior distributions that are positive alongside the associated Savage-Dickey (S-D) ratio between models with evolving and constant $M_{\text{BH}}-M_{\text{bulge}}$ relations. The two models that fixed some / all GSMF parameters (Le03ev / Le00ev) show strong evidence for a positively evolving $M_{\text{BH}}-M_{\text{bulge}}$ amplitude. Models that sampled all 11 GSMF parameters (Le11ev and LM11ev) did not converge to an equally constrained value for α_z . These two models return lower values of α_z overall and are consistent with no significant evolution in the $M_{\text{BH}}-M_{\text{bulge}}$ amplitude.

calculations we present the results from fits to the first 5 frequency bins. Our conclusions are not sensitive to the number of frequency bins we fit to.

3. RESULTS

A summary of the results for the posterior values for α_z are shown in Table 2 and Figure 1. The best-fit spectra for all our models are presented in Figure 3. We find that, in general, a large number of massive SMBHs are needed to reproduce the GWB. When α_z is allowed to vary, the majority of the posterior distribution is positive with a median value of $\alpha_z \sim 0.94$ across all models and $\alpha_z \sim 1.04$ for models with statistically significant evolution. We additionally find that, for models with α_z fixed to be 0, this high number density of massive SMBHs can be modeled either through a top-heavy GSMF (between 0.2 to 3 dex higher in number density for $M_* \geq 10^{11} M_\odot$ and $z > 1$ compared to the observed GSMF, see Figures 4 and 5) or a high $M_{\text{BH}}-M_{\text{bulge}}$ amplitude (with α_0 typically $\sim 8.89 \pm 0.11$ compared to the locally observed value of 8.69, J. Kormendy & L. C. Ho 2013). We first present our full-sample model containing posterior distributions and best-fit spectra for all 29 (30 with α_z) parameters. Then, to highlight the effects of the degeneracy between parameters, we repeat this process with a subset of sampled parameters.

In section 3.4 we present our analysis of the GSMF parameters which we then further discuss in section 4.

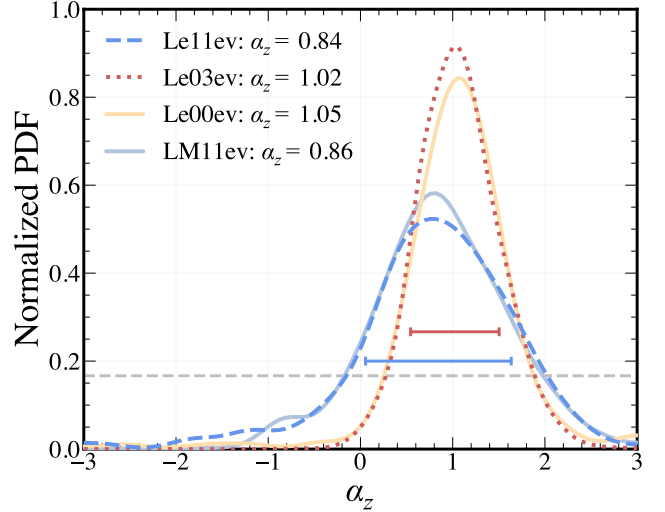


Figure 1. Here we show the four posterior distributions for α_z from our models. The blue and red horizontal lines indicate the 68% confidence region for Le11ev and Le03ev. The gray dashed line shows our uniform prior. These are functionally identical to that of LM11ev and Le00ev respectively. In each distribution 87.2% - 99.3% of values are positive, indicating a moderate to strong positive evolution in the $M_{\text{BH}}-M_{\text{bulge}}$ amplitude. The posterior distributions for our models fall into two categories: (i) A wide range of α_z values with a significant (greater than 10%) fraction of the distribution falling below $\alpha_z = 0$ and (ii) A very narrow, nearly symmetrical, distribution of α_z values with only a negligible (under 5%) fraction of the distribution sitting below $\alpha_z = 0$. This first category corresponds to models that sampled all 11 GSMF parameters (Le11ev and LM11ev), these distributions, while largely positive, are consistent with no significant redshift evolution of the $M_{\text{BH}}-M_{\text{bulge}}$ relation. The latter category, however, show strong evidence for a positive $M_{\text{BH}}-M_{\text{bulge}}$ amplitude evolution. The distributions from this second category had some or all of the GSMF parameters fixed (Le03ev and Le00ev) in the prior set up. With fewer degrees of freedom these models converged to higher values of α_z to a higher degree of confidence suggesting a better constraint for the $M_{\text{BH}}-M_{\text{bulge}}$ amplitude evolution than the larger models. This is indicative of the degeneracy between the GSMF and $M_{\text{BH}}-M_{\text{bulge}}$ parameters in our models.

3.1. Full-Sample Models

Here we present the results of models that sampled all 29 (30 with α_z) parameters. First we describe the outcome of the models that used our fiducial GSMF from J. Leja et al. (2020), then we present the impact of our test cases for explicitly evolving GSMF based on E. R. Liepold & C.-P. Ma (2024).

3.1.1. Le11ne and Le11ev

For the majority of parameters, the posterior distributions recover the priors for both Le11ne and Le11ev.

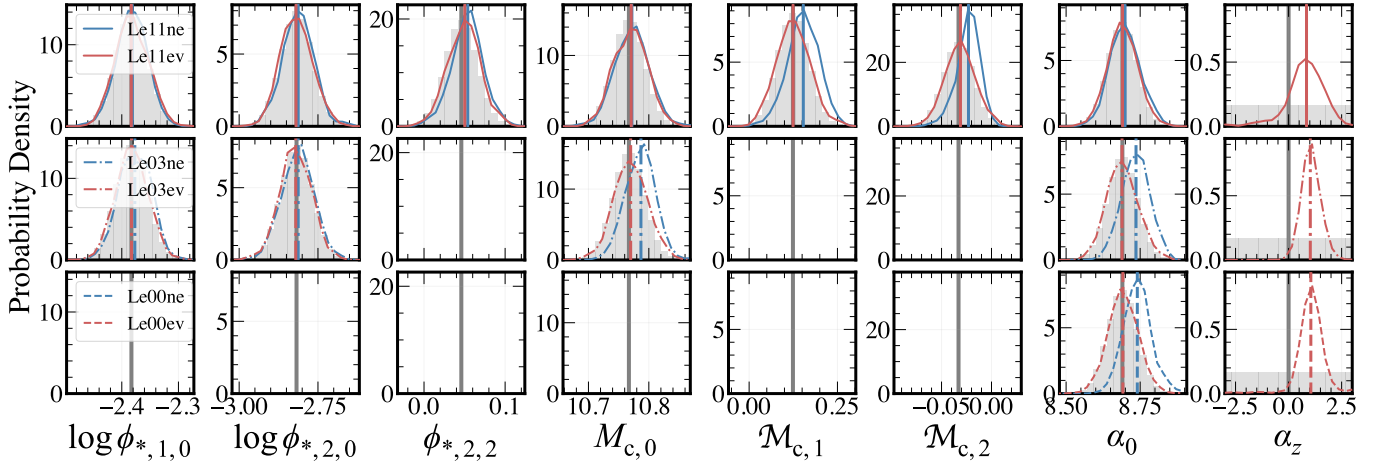


Figure 2. The marginalized posterior distributions for each of the evolving (red) and non-evolving (blue) models. The priors are represented by the gray histograms in each panel and the gray vertical lines indicate the fiducial values. Each row represents a different evolving / non-evolving $M_{\text{BH}}-M_{\text{bulge}}$ model pair—*top*: Le11ne and Le11ev, *middle*: Le03ne and Le03ev, *bottom*: Le00ne and Le00ev. In the case where a parameter was fixed, there is no histogram and only the vertical line is shown. All three posterior distributions for α_z (right-most column) demonstrate a preference for positive values. The α_z posterior is relatively broad for the top row (Le11ev), but when the evolutionary GSMF parameters are fixed (Le03ev, middle row) the distribution shifts towards higher values and also narrows. When only the local GSMF parameters were sampled, but α_z was fixed to 0 (Le03ne), the posterior distributions deviated from the priors, not only for GSMF parameters (e.g. $M_{c,0}$, $M_{c,1}$, and $M_{c,2}$), but also for α_0 . When α_z was allowed to vary, the posteriors recover the prior GSMF parameters. Additionally, when any number of the GSMF parameters are fixed (bottom two rows, Le03ev and Le00ev), the $\alpha_z = 0$ models return high posterior values for the local $M_{\text{BH}}-M_{\text{bulge}}$ amplitude, α_0 . This is indicative of the degeneracy between increasing galaxy number density and increasing the $M_{\text{BH}}-M_{\text{bulge}}$ amplitude (either locally and/or at high- z). We also see little change between α_0 and α_z posteriors in the middle and lower rows suggesting that fixing the three local GSMF parameters (Le00ev) does not have a further affect over fixing only the evolutionary parameters. Overall, the models that allow the $M_{\text{BH}}-M_{\text{bulge}}$ relation to evolve are otherwise in better agreement with observational constraints for the GSMF and local $M_{\text{BH}}-M_{\text{bulge}}$ amplitude and have posterior distributions for α_z that are between 87 and 99% positive.

In the top row of Figure 2 we highlight 8 parameters from these models; complete corner plots can be found in Appendix B. The non-evolving model, Le11ne shows slight deviations towards higher values for three of the the GSMF characteristic mass and normalization evolutionary parameters ($\phi_{*,2,2}$, $M_{c,1}$, and $M_{c,2}$). The two posterior distributions with the largest deviations from the priors are both of the evolutionary parameters for the characteristic stellar mass. When the $M_{\text{BH}}-M_{\text{bulge}}$ relation is allowed to evolve, the posterior distributions for Le11ev are more consistent with the priors for all GSMF parameters, though there is still a mild offset in the same direction as Le11ne for $\phi_{*,2,2}$. The posterior distribution for α_z is 87.2% positive with a median value of 0.85. A Savage-Dickey ratio test in favor of the evolving model returns a value of 1.3, which indicates that this fit is consistent with no $M_{\text{BH}}-M_{\text{bulge}}$ evolution.

The local GSMF values are recovered in both models, but the non-evolving model posteriors return generally larger values for the M_c evolutionary parameters. Notably, 93% of the posterior distribution for $M_{c,2}$ is greater than the prior median and 47% of the distribution falls above the prior 1σ upper limit. Higher values

for $M_{c,1}$ and $M_{c,2}$ produce greater number densities of galaxies at higher redshifts, while maintaining consistency with the fiducial local number density. In particular, larger values for the characteristic mass produce more massive galaxies and therefore a greater number of massive SMBHs.

Figure 4 (see also Fig. 5) compares the GSMFs from J. Leja et al. (2020) to the GSMF implied by the median posterior values from Le11ne and Le11ev. In the local universe, all three GSMFs are in good agreement. By redshift 2, both GSMFs from Le11ne and Le11ev lie above the observed values, but Le11ev is consistent, within error bars with J. Leja et al. (2020). The difference between the GSMFs becomes larger with redshift with Le11ev remaining consistent with the observed GSMF while Le11ne is 0.5 to 2 orders of magnitude greater for galaxies with $M_* \geq 10^{10.5} M_\odot$ at $z = 3$. These massive galaxies are the hosts to the SMBHs in the mass range that dominates the GWB signal ($M_{\text{BH}} > 10^9 M_\odot$ G. Agazie et al. 2023b). When predicting SMBH masses using the local $M_{\text{BH}}-M_{\text{bulge}}$ relation, to increase the amplitude of the modeled GWB, we need an increased number density of these massive

galaxies compared to the fiducial model. Alternatively, an evolving $M_{\text{BH}}-M_{\text{bulge}}$ relation offers a way to increase the number density of the most massive SMBHs without any changes to the galaxy population or the locally observed SMBH–galaxy relation. This suggests that the best-fit parameters for models with an evolving $M_{\text{BH}}-M_{\text{bulge}}$ amplitude are more consistent with observational constraints than non-evolving models.

3.1.2. *LM11ne and LM11ev*

We find an anti-correlation between the strength of the GSMF evolution we assume and the resulting GWB amplitude. A strongly evolving GSMF (larger values of $M_{c,i}$) predicts lower mass densities of galaxies relative to a weakly evolving GSMF (lower values of $M_{c,i}$). The strongly evolving GSMFs also, therefore, produce lower number densities of the most massive SMBHs which then produces to lower GWB amplitudes.

Despite the greatly increased number density of local galaxies in this model, the strongly evolving GSMF produces a GWB spectrum that is only marginally greater in amplitude than the fiducial model. In fact, the posterior distributions, using the strongly evolving [E. R. Liepold & C.-P. Ma \(2024\)](#) GSMF (with its much higher number density of galaxies with $M_{\star} \geq 10^{11.5} M_{\odot}$), display similar behavior to that of Le11ne and Le11ev. That is, the GSMF posteriors for models without $M_{\text{BH}}-M_{\text{bulge}}$ evolution tend towards greater number densities of high-mass galaxies for $z \gtrsim 1$. The GSMF posteriors recover the priors when $M_{\text{BH}}-M_{\text{bulge}}$ evolution is allowed and the posterior distribution for α_z is nearly identical to that of Le11ev (see Figure 1).

In Figure 5 we compare the prior and posterior GSMFs for all full-sample models. We see that the galaxy number densities for $1 \lesssim z < 3$ are roughly equivalent for Le11ne and LM11ne (similarly for Le11ev and LM11ev). We see a more significant difference between models that have an evolving or static $M_{\text{BH}}-M_{\text{bulge}}$ relation than between models with different prior GSMFs (further discussed in section 3.4). This result suggests that, to reproduce the GWB amplitude, we need a significantly greater number density of galaxies than we currently observe, not only locally, but at least out to $z = 3$. We discuss the physical implications and feasibility of this model further in section 4.

While the local GSMF measured by [E. R. Liepold & C.-P. Ma \(2024\)](#) offers valuable insight into the local galaxy population and the limits of volume-limited surveys, we do not find that this local increase in galaxy number density is sufficient to reproduce the observed GWB spectrum. The difference between our result and the what [E. R. Liepold & C.-P. Ma \(2024\)](#) find is a direct

result of the assumptions made about binary hardening mechanisms in our respective calculations. For their estimate of the GWB amplitude, [E. R. Liepold & C.-P. Ma \(2024\)](#) follow the methods of [G. Sato-Polito et al. \(2024\)](#) and [E. S. Phinney \(2001\)](#). This model includes only the effect of gravitational wave-driven SMBH binary hardening, which produces a power-law spectrum. In this work, we assume that binaries can also harden through dynamical friction and stellar scattering. The effect of these additional hardening pathways is to change the shape of the overall spectrum and to lower the amplitude. While keeping all other parameters constant, the change in shape and amplitude has the greatest impact at the low-frequency end of the spectrum ($f \lesssim 10\text{nHz}$, e.g., see lower-right panel of Figure 4 in [G. Agazie et al. 2023a](#)). The shape of the spectrum, when including these additional hardening mechanisms, provides better fits to the data across the observed range of frequencies than the gravitational wave-only model ([G. Agazie et al. 2023a](#)).

3.2. *Fixed GSMF Evolution Models: Le03ne and Le03ev*

The first of the sub-models that we discuss are Le03ne and Le03ev. Each of these is identical to Le11ne and Le11ev respectively except the six evolutionary parameters ($\phi_{*,1,1}$, $\phi_{*,1,2}$, $\phi_{*,2,1}$, $\phi_{*,2,2}$, $M_{c,1}$, and $M_{c,2}$) alongside α_1 and α_2 for the GSMF are fixed to the posterior values given by [J. Leja et al. \(2020\)](#). To focus on the degeneracy between GSMF and $M_{\text{BH}}-M_{\text{bulge}}$ parameters we additionally fixed all parameters for galaxy merger rates and bulge fractions to their fiducial values. These models, therefore, sample a total of 8 parameters (9 with α_z).

When sampling from all 11 GSMF parameters, the posteriors for the model that did not allow for $M_{\text{BH}}-M_{\text{bulge}}$ evolution (Le11ev) recovered the priors for the local GSMF values while only the evolutionary parameters deviated. Now, since these evolutionary parameters were fixed, the local GSMF posterior for characteristic mass is distributed towards greater values. Unlike before, this model also returns a posterior distribution with generally larger values of the $M_{\text{BH}}-M_{\text{bulge}}$ amplitude than the prior. An increase to either the characteristic galaxy mass or the $M_{\text{BH}}-M_{\text{bulge}}$ amplitude can generate the top-heavy BHMFs necessary to reproduce the observed GWB. A moderate (within 1σ) increase to both parameters, on the other hand, allows for massive SMBH populations to be modeled without deviating too far from either one parameter. This result is consistent with what [G. Agazie et al. \(2023b\)](#) found—to match the GWB either a large number of parameters in the fiducial

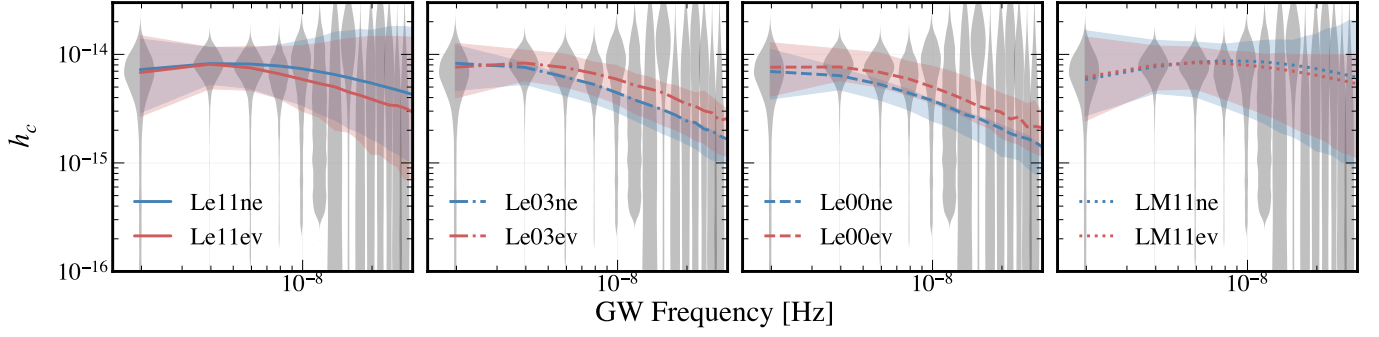


Figure 3. The GWB spectra associated with the best-fit parameters from our 8 models fit to the first five frequency bins. In all four panels, the spectrum from the evolving $M_{\text{BH}}-M_{\text{bulge}}$ models are in good agreement with the data though we note that the likelihood value for Le00ev is the lowest of the 8 models (discussed further in section 3.4). There are some differences between the slope of the high-frequency end, but this portion of the spectrum is poorly constrained and it is not possible to distinguish between goodness of fit in this regime at this time. When all GSMF parameters are sampled (left- and right-hand panels, Le11ne and LM11ne), the spectra are nearly identical between the evolving and non-evolving models. The models with some/all GSMF parameters fixed (Le03ne and Le00ne) show more significant differences between the evolving and non-evolving models. For these models, those that allowed α_z to vary are consistently in better agreement with the data than the fixed $\alpha_z = 0$ counterparts indicating that these evolving models are a better description of the GWB than their non-evolving counterparts.

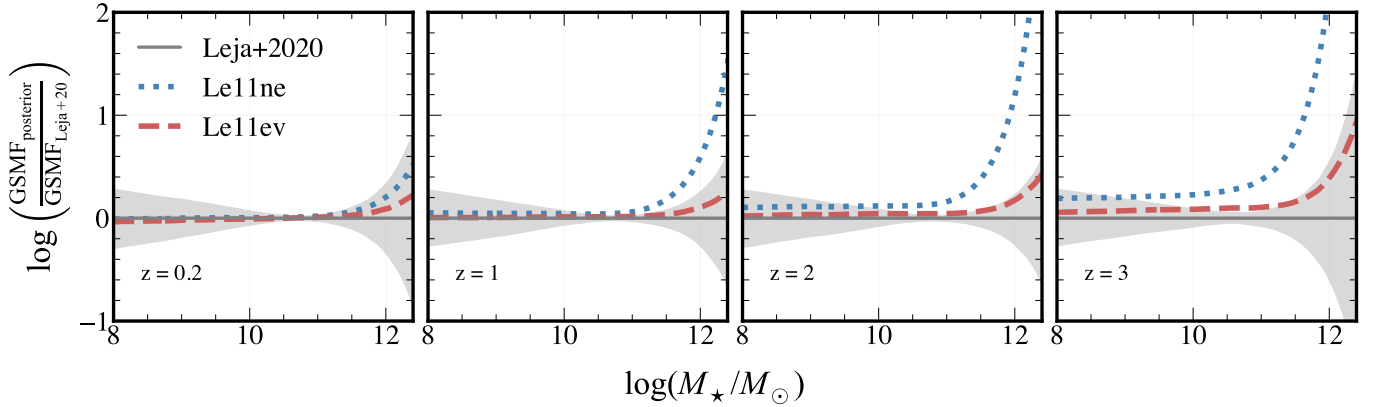


Figure 4. Here we plot the difference between the posterior GSMF from both the evolving (Le11ev, red dashed) and non-evolving (Le11ne, blue dotted) $M_{\text{BH}}-M_{\text{bulge}}$ model and the observed GSMF from J. Leja et al. (2020). The light gray region represents the error in the GSMF from J. Leja et al. (2020). We compare the models only within the redshift range used in J. Leja et al. (2020) $0.2 < z < 3$. We see that, when the $M_{\text{BH}}-M_{\text{bulge}}$ relation is not allowed to evolve, the GSMF shows higher number densities of high-mass galaxies with an increasing discrepancy as redshift increases. This difference is highest for galaxies with $M_* > 10^{11}$ though by $z = 3$ the posterior GSMF from Le11ne is inconsistent with the observed GSMF at all masses $M_* > 10^9$. When the $M_{\text{BH}}-M_{\text{bulge}}$ amplitude is allowed to evolve, however, the posterior GSMF is consistent within the uncertainties of the observed GSMF though with a minor positive offset. This is evidence that our best-fit models with an evolving $M_{\text{BH}}-M_{\text{bulge}}$ amplitude are in better agreement with observational constraints for galaxy number density than the non-evolving models.

model need to change by a small amount, or a very small number of parameters must be significantly different.

When the $M_{\text{BH}}-M_{\text{bulge}}$ relation is allowed to evolve, the posterior distributions for all GSMF parameters are in good agreement with the priors, even more than with Le11ev. Interestingly, the distribution for α_z , for this model, is 99.3% positive with a Savage-Dickey ratio of 24.6. The standard deviation of this distribution is also significantly reduced indicating a higher confidence of positive evolution.

Nearly all samples from the model that did not include $M_{\text{BH}}-M_{\text{bulge}}$ evolution tend towards lower GWB amplitudes. In the second panel of Figure 3 we see that the shape of the GWB spectrum is nearly straight with the best fit model lying below the bulk of the data for the majority of the frequency bins. The Le03ev model, on the other hand, while lower in GWB amplitude than Le11ev at the high frequency end, is still consistent with the PTA data.

3.3. Fixed GSMF Models: *Le00ne* and *Le00ev*

Finally, we present the smallest subset of our models, which only sample the three hardening parameters, the $M_{\text{BH}}-M_{\text{bulge}}$ amplitude, and α_z (for *Le00ev*). These models fix all 11 GSMF parameters to their fiducial values from [J. Leja et al. \(2020\)](#) so the local and high- z GSMF cannot vary for these models.

This subset of models returns a posterior α_z distribution that is 96.8% positive with a Savage-Dickey ratio of 5.2. In this case, the posterior distribution for $M_{\text{BH}}-M_{\text{bulge}}$ amplitude recovers the prior almost exactly. For the non-evolving model, to reproduce high SMBH masses, a greater overall $M_{\text{BH}}-M_{\text{bulge}}$ amplitude is required. This result demonstrates how the models will trend more strongly towards positive values of α_z as the other options for increasing the number density of massive SMBHs are removed. When the option for evolution is also removed, the posteriors will deviate strongly from the priors for parameters that are influential on the predicted SMBH number density.

The GWB spectra share similar characteristics to the *Le03ne* and *Le03ev* models with the non- $M_{\text{BH}}-M_{\text{bulge}}$ evolving models consistently lying below the majority of the PTA data and the evolving $M_{\text{BH}}-M_{\text{bulge}}$ models falling closer to the center of the violins in more bins, but lying slightly above the median. We note that the best-fit spectrum for *Le03ne* has the lowest likelihood of all 8 spectra, an effect we detail further in [Appendix C](#).

3.4. Influence of the GSMF

In this section we present the posterior GSMFs in two ways. We show the posterior GSMFs over-plotted with the corresponding prior GSMF for full GSMF sample models in [Figure 5](#) for visual comparison. We then quantify the number density increase relative to [J. Leja et al. \(2020\)](#), which we plot versus the corresponding $\alpha(z)$ posterior median to demonstrate the degeneracy between these quantities in [Figure 6](#).

In [Figure 5](#) we can see that the posterior GSMF from *Le11ne* and *LM11ne* generally have higher number densities than the fiducial model. This offset is most extreme for the *LM11ne* GSMF which is to be expected since the fiducial GSMF for this model started with a higher number density than the [J. Leja et al. \(2020\)](#) GSMF for $z < 1$. Both of these GSMFs are greater in number density than their respective fiducial model and the fixed $\alpha_z = 0$ counterpart. Though we highlight the most extreme examples here, this is a trend across models that the fixed $\alpha_z = 0$ models require a greater number density of (especially the most massive) galaxies.

Because the GSMF is defined by up to 11 parameters in our models, the degeneracy between $\alpha(z)$ and any given GSMF parameter is not very strong. There is, however, considerable degeneracy between the $M_{\text{BH}}-M_{\text{bulge}}$ evolution and an increased number density of galaxies. To further demonstrate this degeneracy we define the quantity Ξ to be the integrated difference of the number density of galaxies between two models (see [equation 6](#)). We integrate over $11 < \log M_* < 13$ in mass and $0.5 \leq z \leq 3$ in redshift and note that trend of the results of this analysis are not sensitive to the bounds of our integral. We chose to omit $0 < z < 0.5$ in the integration range for clarity, including this range only results in a constant positive offset in Ξ for both *LM11ne* and *LM11ev*. We additionally normalize Ξ such that all our values lie between 0 and 1; $\Xi = 0$ indicates that the posterior GSMF is equivalent to the prior GSMF across our integration range (which is the case for both *Le00ne* and *Le00ev*). The Ξ parameter encapsulates the “boost” in galaxy number density and is analogous to the way $\alpha(z)$ encodes the changing $M_{\text{BH}}-M_{\text{bulge}}$ amplitude.

$$\Xi = \iint [\phi_{\text{posterior}}(M, z) - \phi_{\text{Leja}+20}(M, z)] M dM dz \quad (6)$$

In [Figure 6](#) we plot Ξ against the $M_{\text{BH}}-M_{\text{bulge}}$ amplitude at a fixed redshift $\alpha(z = 1.5)$, locally all values of $\alpha(z)$ are equivalent and the value of z we choose only shifts the evolving $M_{\text{BH}}-M_{\text{bulge}}$ models left or right on the x-axis. The color differentiates evolving (red) models from non-evolving (blue) and the marker styles show the pairs of models with the same prior set up aside from $M_{\text{BH}}-M_{\text{bulge}}$ evolution (i.e., each marker style appears twice, one on red and one on blue). The clear negative trend demonstrates the degeneracy between an increased number density of galaxies and an increased SMBH–galaxy mass ratio in our posterior models. In the cases where the GSMF was allowed to vary, the evolving models (*Le11ev*, *Le03ev*, *Le00ev*, and *LM11ev*) have a lower value for Ξ and a higher value for $\alpha(z = 1.5)$ than their non-evolving counterparts (*Le11ne* and *Le03ne*). These models follow the same trend, but are additionally boosted relative to the fiducial [J. Leja et al. \(2020\)](#) GSMF by design (as described in [section 2.3](#) and [Appendix A](#)). The only outlier to this trend is *Le00ne*. The best-fit likelihood value for this model is several orders of magnitude smaller than for other models (represented by the size of the points) and therefore its location on the plot is not an accurate reflection of the overall trend. Therefore we conclude that the high number density of massive SMBHs, required to reproduce the GWB, can be produced either by a large increase to galaxy number

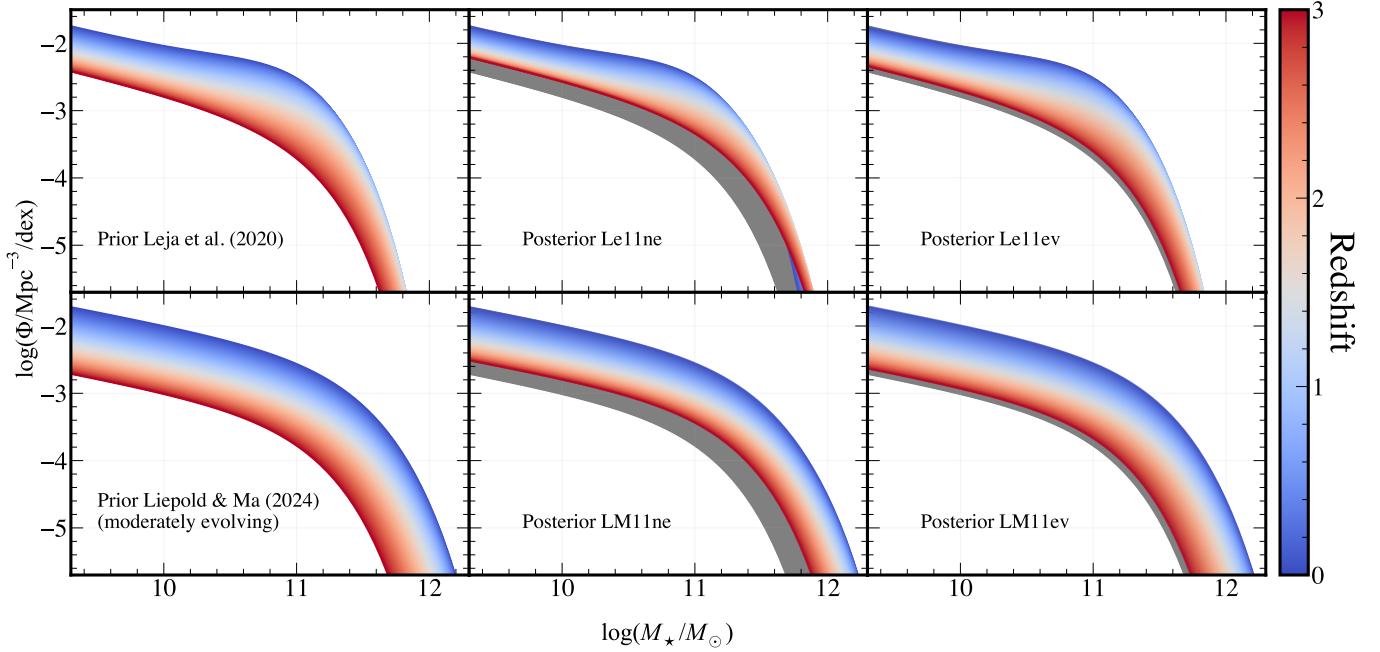


Figure 5. *Top left:* The prior GSMF from [J. Leja et al. \(2020\)](#). *Top middle:* The posterior GSMF for Le11ne. *Top right:* The posterior GSMF for Le11ev. *Bottom:* Same as top row, but for models based on our moderately evolving version of the [E. R. Liepold & C.-P. Ma \(2024\)](#) GSMF. We see that, in both middle plots, the models that have $\alpha_z = 0$ require a large number density of galaxies relative to their respective fiducial model. Despite the increased local number density, the posterior GSMF from LM11ne returns a greater number density for $z = 3$ compared to the [J. Leja et al. \(2020\)](#) GSMF. The prior for this model had a similar number density to that of [J. Leja et al. \(2020\)](#) in this redshift range, by design. The number densities for $2 \lesssim z \lesssim 3$ are similar between the two posterior models with $\alpha_z = 0$. This means that, to reproduce the GWB without an evolving $M_{\text{BH}}-M_{\text{bulge}}$ amplitude, we need a significantly higher number density of massive galaxies across out to $z \sim 3$. For both models that allowed α_z to vary (right-most panels) the posterior GSMFs are only negligibly different from the priors and the corresponding median posterior values for α_z are similar (see Figure 1 and Table 2) implying that the locally increased number density for LM11ev does not sufficiently increase the GWB amplitude without additionally increasing the high- z GSMF.

density (GSMF), a large increase to the SMBH–galaxy mass ratio, or a moderate increase to both.

The models that fix some / all GSMF parameters converge to higher values of α_z with a greater degree of confidence. The Le03ev model only fixed the evolutionary parameters from [J. Leja et al. \(2020\)](#) and sampled the local GSMF values. The posteriors for this model recovered the local GSMF and $M_{\text{BH}}-M_{\text{bulge}}$ parameters while its counterpart model, with α_z fixed to 0, (Le03ne) did not. This suggests that the GWB free-spectrum is well described by a SMBH population as predicted from an evolving $M_{\text{BH}}-M_{\text{bulge}}$ relation and the galaxy number density given by the GSMF due to [J. Leja et al. \(2020\)](#). The GWB spectrum is equally well described by an unchanging $M_{\text{BH}}-M_{\text{bulge}}$ relation if, and only if, the GSMF is significantly higher in number density (for $M_* > 10^{11.5} M_\odot$), not only locally, but also out to z as high as 3, which is not well supported by observational data (e.g., [A. Muzzin et al. 2013](#); [A. R. Tomczak et al. 2014](#); [I. Davidzon et al. 2017](#); [P. Behroozi et al. 2020](#)),

though it is not entirely ruled out (e.g., [J. Moustakas et al. 2013](#); [A. H. Wright et al. 2018](#)).

3.5. Black Hole Number Density

In Figure 7 we present the BHMFs resulting from our models for $0.25 \leq z \leq 2$. We additionally plot the posterior single SMBH functions from Figure 13 in [G. Agazie et al. \(2023b\)](#) and our fiducial BHMF for comparison. The BHMFs for evolving models using the [J. Leja et al. \(2020\)](#) GSMF (Le11ev, Le03ev, and Le00ev) are nearly identical to each other and so we plot one BHMF that is the median of all three models. We compare this to the posterior BHMF from LM11ev and find that the BHMFs are broadly consistent for $z > 0.5$, but that of LM11ev is greater in number density for the most massive SMBHs for $z < 0.5$. This is to be expected since this is the same behavior seen in the respective GSMFs.

We also show the median BHMF for the fixed $\alpha_z = 0$ models, Le11ne and Le03ne, (excluding Le00ne due to its low likelihood). This BHMF has a lower number density than that of the evolving models across the entire

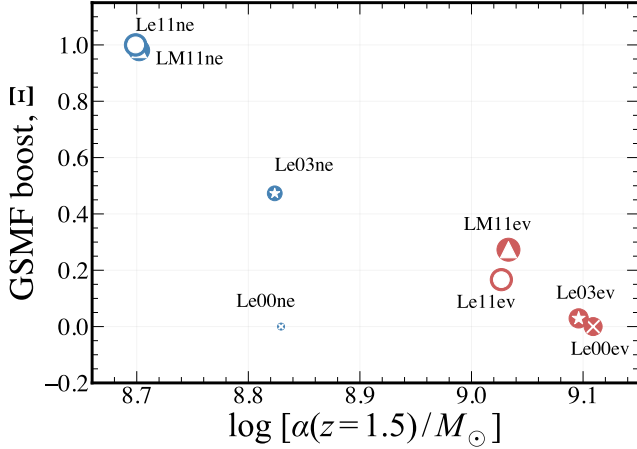


Figure 6. The quantity, Ξ , represents the normalized number density “boost” in a given posterior GSMF relative to the corresponding fiducial GSMF for $11 < \log M_{\star} < 13$ and $0.5 < z < 3$. $\Xi = 0$ means the two GSMFs are equivalent, a positive value of Ξ corresponds to an increased number density relative to the fiducial model across our integration range, all Ξ values were normalized to a maximum of 1. Red points are for models that allow the $M_{\text{BH}}-M_{\text{bulge}}$ relation to evolve and blue points fixed α_z to be 0. The size of the points corresponds to the log likelihood value of the best-fit GWB spectrum (i.e., larger circles are better matches for the GWB). Each model pair shares a marker style overlaid in white (e.g., Le11ne and Le11ev are blue and red circles with stars). There is a clear negative correlation between pairs and also across all models. This demonstrates the degeneracy between an increased number density of galaxies and an increased SMBH–galaxy mass ratio. This degeneracy exists because both are valid pathways to producing the high number density of massive SMBHs implied by the GWB.

mass range for $z > 1$. This BHMF is more similar to the fiducial BHMF for low redshifts, but has a boosted number density which increases with redshift. This increasing positive offset is reflective of the GSMF posteriors and the increased number density of galaxies in the non-evolving best-fit models (for Le11ne and Le03ne).

Generally, all posterior models have a higher number density of SMBHs relative to the fiducial model across all redshift bins while evolving models typically have the highest number densities in a given bin.

4. DISCUSSION

Our results suggest that either the $z = 0$ $M_{\text{BH}}-M_{\text{bulge}}$ relation does not apply at higher redshift or galaxy observational surveys drastically underestimate the number of massive galaxies at all redshifts $z < 3$ either through non-detection of a population or by underestimating masses. The best-fit evolving models indicate a positive offset for the $M_{\text{BH}}-M_{\text{bulge}}$ amplitude in the past. An $M_{\text{BH}}-M_{\text{bulge}}$ amplitude that increases with

redshift ($\alpha_z > 0$) implies a black-hole-first evolution. Some studies have proposed this as a possible formation route stating that kinetic-mode feedback from SMBH accretion disks can impede the star formation within the host galaxy thus leading to a delayed stellar mass increase (M.-Y. Zhuang & L. C. Ho 2023), also known as black hole “dominance” (M. Volonteri 2012). In the opposite case, decreasing amplitude at high- z may be indicative of radiative-mode feedback, where UV radiation from star formation prevents gas from sinking to the center of the galaxy therefore postponing SMBH accretion (M.-Y. Zhuang & L. C. Ho 2023). Our results support the black hole dominance model of SMBH–galaxy coevolution. The value for the $M_{\text{BH}}-M_{\text{bulge}}$ amplitude evolution we find $\alpha_z = 1.04 \pm 0.5$ is consistent with several observational (X. Ding et al. 2020; F. Pacucci et al. 2023; Y. Zhang et al. 2023; T. S. Tanaka et al. 2025) studies and some theoretical / simulation studies (e.g., J. S. B. Wyithe & A. Loeb 2003; A. Cattaneo et al. 2005; D. J. Croton 2006), but there is a lack of consensus among these studies, especially for the redshifts most relevant for the GWB (e.g., A. Merloni et al. 2010; V. N. Bennert et al. 2011; J. Li et al. 2021; M. Cisternas et al. 2011). Our analysis places the strongest constraints only on the most massive SMBHs ($M_{\text{BH}} \geq 10^8 M_{\odot}$). We cannot firmly differentiate between our power-law evolution and more complex models (such as dual sequence behavior T. Shimizu et al. 2024) nor can we determine whether the evolution is mass-dependent (e.g., A. Hoshi et al. 2024). A complementary follow-up analysis could consider the effect of heavy versus light SMBH seeding models on the low-mass end of the $M_{\text{BH}}-M_{\text{bulge}}$ relation to form a bigger picture of $M_{\text{BH}}-M_{\text{bulge}}$ evolution.

In Figure 8, we show the $M_{\text{BH}}-M_{\text{bulge}}$ amplitude offset ($\Delta \log M_{\text{BH}}/M_{\odot}$) versus redshift predicted by our model alongside measurements from literature. The gray scattered points represent individual galaxies with both stellar and SMBH mass measurements and so we calculate the offset from the local $M_{\text{BH}}-M_{\text{bulge}}$ relation for these objects. The lines each represent a model from papers which provide an explicit functional form or offset for $M_{\text{BH}}-M_{\text{bulge}}$ evolution. The thicker red line and shaded red region represent the median posterior value for α_z and 68% confidence region from our models with statistically significant evolution (Le03ev and Le00ev). We find that our model is most consistent with that from Y. Zhang et al. (2023) (yellow dotted line) though our error bars encompass the models due to J. S. B. Wyithe & A. Loeb (2003) and A. Merloni et al. (2010). We note that both M.-Y. Zhuang & L. C. Ho (2023) and A. Merloni et al. (2010) were careful to account for observational bias (e.g., as described by T. R. Lauer et al.

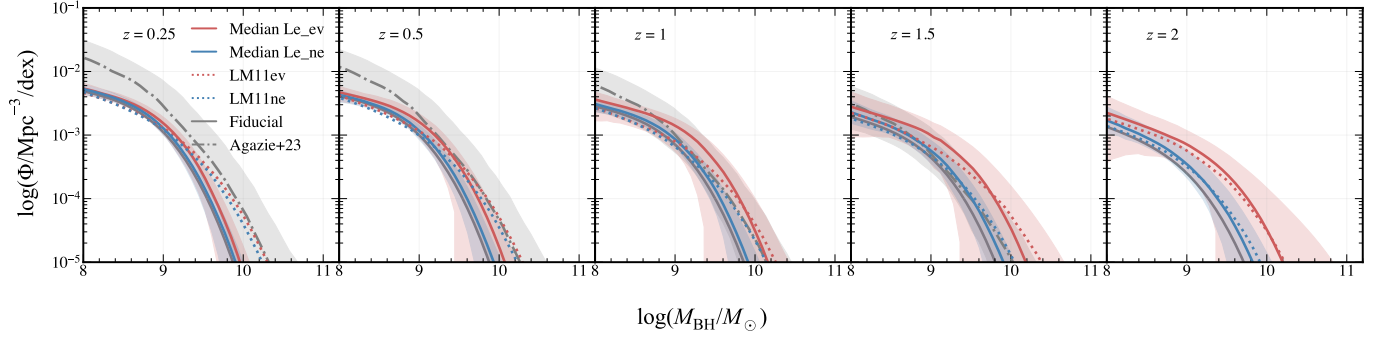


Figure 7. Posterior BHMFs from our best-fit models compared with the fiducial model and the BHMf from G. Agazie et al. (2023b). The red (blue) solid lines represent the median BHMf from all the evolving (non-evolving) models that used the J. Leja et al. (2020) GSMF. Models using the E. R. Liepold & C.-P. Ma (2024) follow this same color convention and are dotted instead of solid. We exclude Le00ne from these calculations because of its low likelihood value. Generally, the models that have an evolving $M_{\text{BH}}-M_{\text{bulge}}$ have higher number densities at higher redshifts compared to the non-evolving counterparts. The models that used the J. Leja et al. (2020) and did not allow for $M_{\text{BH}}-M_{\text{bulge}}$ evolution are mildly positively offset from the fiducial BHMf. This offset increases with redshift reflecting the difference in posterior GSMF evolution.

2007) in their analysis. Our model does not predict as extreme an offset as measured by X. Ding et al. (2020), F. Pacucci & A. Loeb (2024), or M. Yue et al. (2024).

We find $\alpha_z = 1.04 \pm 0.5$ which lies below the value ($\alpha_z \sim 2.07 \pm 0.47$) found by Y. Chen et al. (2024). Y. Chen et al. (2024) perform a similar analysis to the one we present here in which they fit the same data and also use the same fiducial $M_{\text{BH}}-M_{\text{bulge}}$ relation as us. There are two key differences in their model versus ours: (i) the GSMF and (ii) the SMBH binary hardening model. They use the GSMF due to P. Behroozi et al. (2020), which has notably different (both higher and lower) number densities to our fiducial model across the mass and redshift ranges we consider. Because the GSMF they assume is not uniformly offset from ours, the effect on their α_z estimate is not obvious, but this difference is certainly a contributing factor to this discrepancy. Another difference between our models is the hardening prescription for the SMBH binaries. The model they use is a more complex model than we used here (Y. Chen et al. 2020). Differences in binary hardening efficiency can affect the GWB amplitude. We are able to model the GWB using $\alpha_z \sim 2.07$ if we assume a hardening timescale that is much longer than currently supported values (by up to a factor of ten times higher than reported in G. Agazie et al. 2023b). For this work, we assume a constant hardening timescale and the discrepancy between these results is demonstrative of the need for realistic binary hardening models. Future testing with EM studies will be important for placing bounds on hardening timescales. Inferences for SMBH populations from the GWB are sensitive to the underlying models used for galaxy populations. The difference in our results demonstrates the importance for having robust and well-constrained models.

Our analysis here suggests that, if we can reproduce the high GWB amplitude through only changes to the GSMF, then this would require a significantly higher number density of the highest mass galaxies at higher redshifts (at least out to $z = 3$). As they discuss in their paper, the increased number density that E. R. Liepold & C.-P. Ma (2024) find indicates that galaxy surveys are missing out on the population of the most massive galaxies ($M_{\star} \geq 10^{11.5} M_{\odot}$) and/or the mass to light ratios underestimate galaxy mass for this population. Local surveys may miss out on this population of galaxies because the survey area is simply not large enough to include this otherwise rare population. For higher redshifts, however, the survey volume is sufficient to ensure completeness and so the, e.g., COSMOS (C. Laigle et al. 2016) and 3D-HST+CANDELS survey (R. E. Skelton et al. 2014) surveys used in J. Leja et al. (2020) should be representative of the underlying population. This, combined with the abundance of reliable data, would suggest that the posterior GSMF at $z > 1$, needed by our models to match the GWB spectrum, is inconsistent with the true galaxy population. If, however, the initial mass function is bottom heavy, like that assumed by E. R. Liepold & C.-P. Ma (2024) and minimally evolving (and therefore bottom heavy at higher redshifts), then a GSMF like that in the bottom middle panel of Figure 5 could be feasible. In either case, analyses of the GWB are most directly a probe of SMBH properties, so any inferences we draw about the GSMF are several steps removed and are therefore only implicit. It is still useful to discuss the degeneracies with the GSMF in our models, however the GSMF estimates from this study should be treated with caution.

Gravitational wave-based studies, such as this, offer a new probe of SMBH-galaxy- mass scaling relations

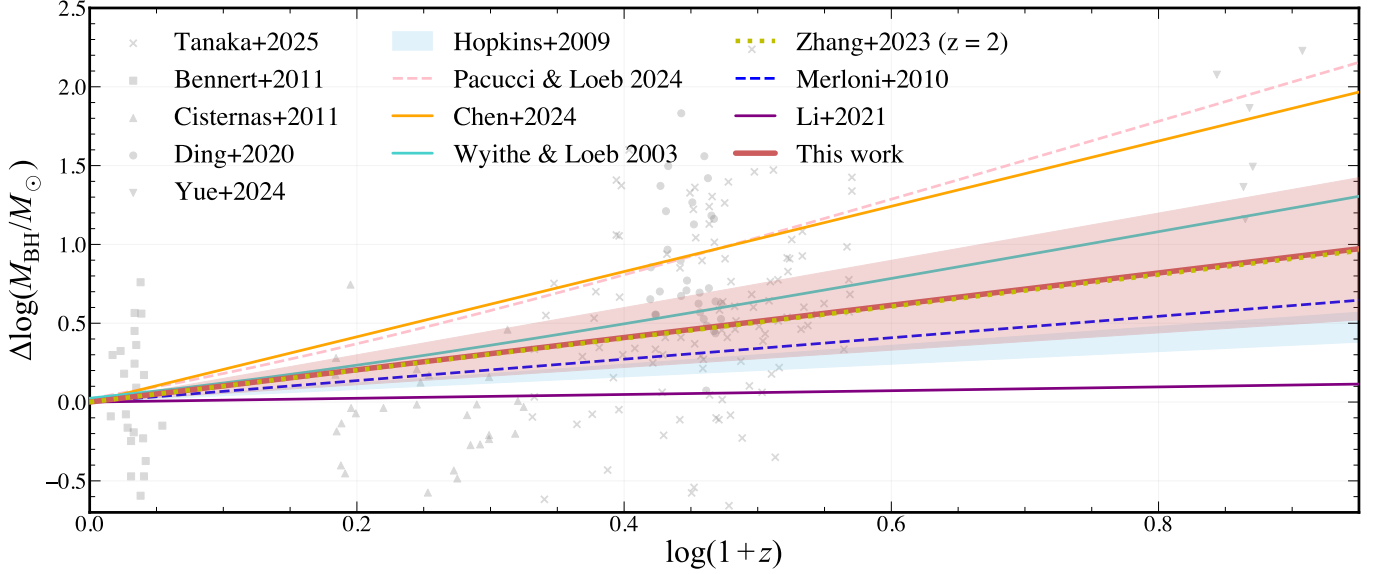


Figure 8. A comparison between different literature estimates of the $M_{\text{BH}}-M_{\text{bulge}}$ relation and our results (thick, solid red line and 68% confidence shaded region). The y-axis is the (log) offset between SMBH mass at a given redshift compared to the local amplitude. For this figure, we only include our models with statistically significant evolution (Le03ev and Le00ev). The gray points represent data while the different lines are fitting results. For Y. Zhang et al. (2023) (yellow dotted) we approximate the evolutionary form based on their reported redshift range and $M_{\text{BH}}-M_{\text{bulge}}$ offset. Our analysis favors an intermediate positive evolution which is nearly identical to that of Y. Zhang et al. (2023) and similar to those of J. S. B. Wytthe & A. Loeb (2003) and A. Merloni et al. (2010). Our model does not predict offsets as great as F. Pacucci & A. Loeb (2024), M. Yue et al. (2024), or Y. Chen et al. (2024).

that can complement observational studies. Broadly speaking, there are two ways to observationally infer the SMBH mass function over cosmic time using only electromagnetic data: (i) BH mass scaling relations combined with observations of galaxies and (ii) models of Eddington ratio distributions combined with observations of AGN luminosity functions. These two methods have inferred incompatible SMBH mass functions, with galaxy-observation methods predicting higher densities than AGN-observation methods. A series of works (F. Shankar et al. 2016; E. Barausse et al. 2017; F. Shankar et al. 2019) proposed a potential solution whereby the (non-evolving) mass scaling relations had much lower amplitude (possibly a result of unsubstantiated measurement biases) to lower the galaxy-observation results to be in line with the AGN-observation results. Our work here shows that the GWB spectrum is generally in line with the galaxy-observation results. Not only are the measured scaling relations not too low at $z = 0$, they are, if anything, higher amplitude at higher redshift, something which is also noted by other studies (e.g., G. Sato-Polito et al. 2024; E. R. Liepold & C.-P. Ma 2024). One as yet under-explored possibility to reconcile these two observational results is that radiative efficiencies are lower by a factor of 2 – 5 than typically assumed for the brightest AGN. This is outside the scope of this paper, but will be investigated in future studies.

Our analysis of the $M_{\text{BH}}-M_{\text{bulge}}$ relation focused on evolution of the amplitude, however it is possible that the relation may be evolving in other ways. Recent work has suggested that a variety of growth pathways are likely to be relevant within galaxy populations and that they are encoded in the intrinsic scatter (M.-Y. Zhuang & L. C. Ho 2023; B. A. Terrazas et al. 2024; H. Hu et al. 2025; J. H. Cohn et al. 2025) where the local $M_{\text{BH}}-M_{\text{bulge}}$ relation acts as a sort of “attractor” for SMBH–galaxy pairs as they evolve. This concept is not new (e.g., C. Y. Peng 2007; M. Hirschmann et al. 2010; A. Merloni et al. 2010; K. Jahnke & A. V. Macciò 2011), but has seen a lot of new analysis, especially in the last two years. In particular, M.-Y. Zhuang & L. C. Ho (2023) conducted a study of $z \leq 0.35$ AGNs and found that the scatter in the $M_{\text{BH}}-M_{\text{bulge}}$ relation is greater in the early universe, a finding substantiated recently by both gravitational wave and simulation analyses (e.g., E. C. Gardiner et al. 2023; B. A. Terrazas et al. 2024). Furthermore, J. Li et al. (2025) measured the SMBH–galaxy mass ratios for AGN at $z \sim 3 - 5$ and found that they are consistent with the local population. Results such as theirs could be indicative of an increased scatter in the $M_{\text{BH}}-M_{\text{bulge}}$ relation outside the local universe. Biased observations of a high-scatter $M_{\text{BH}}-M_{\text{bulge}}$ relation could appear, artificially, as an inflated amplitude. Future GWB studies similar to this will provide valu-

able insights into alternative evolutionary forms of the $M_{\text{BH}}-M_{\text{bulge}}$ relation.

It is also possible that a scaling relation not based on galaxy mass may more accurately reproduce the highest-mass SMBH number density. It has been shown that the $M_{\text{BH}}-M_{\text{bulge}}$ and $M_{\text{BH}}-\sigma$ relations predict different BHMFs outside the local universe (C. Matt et al. 2023) and that this has an impact on the predicted GWB amplitude (J. Simon 2023). On the other hand, N. J. McConnell & C.-P. Ma (2013) found that both the $M_{\text{BH}}-M_{\text{bulge}}$ and $M_{\text{BH}}-\sigma$ relations “saturate” towards the highest masses, underpredicting SMBH masses for the largest bright cluster galaxies. And an analysis by G. Sato-Polito et al. (2024) finds that neither of the local relations can reproduce the high GWB amplitude. In either case, there is strong evidence to suggest that the local $M_{\text{BH}}-M_{\text{bulge}}$ relation was different in the past in some way, and multimessenger studies such as this are an exiting route towards characterizing SMBH–galaxy coevolution.

5. SUMMARY AND CONCLUSIONS

In this work we implemented an evolving $M_{\text{BH}}-M_{\text{bulge}}$ model which improves our ability to reproduce the GWB while maintaining consistency with astrophysically constrained models. We adapted the HOLODECK semi-analytic model to test for evolution in the $M_{\text{BH}}-M_{\text{bulge}}$ relation and fit models to the GWB free-spectrum from G. Agazie et al. (2023a). Our results show mild to strong preference for a positive evolution in the $M_{\text{BH}}-M_{\text{bulge}}$ amplitude. When modeling the $M_{\text{BH}}-M_{\text{bulge}}$ relation as $M_{\text{BH}} = \alpha_0(1+z)^{\alpha_z}(M_{\text{bulge}}/10^{11} M_{\odot})^{\beta_0}$ we find that $\alpha_z = 1.04 \pm 0.5$.

We also studied the degeneracy between the GSMF and $M_{\text{BH}}-M_{\text{bulge}}$ relation. The GWB requires massive SMBHs and we find that this population can be modeled with a top-heavy GSMF (which becomes a top-heavy BHMF via the local $M_{\text{BH}}-M_{\text{bulge}}$ relation) or an increased $M_{\text{BH}}-M_{\text{bulge}}$ amplitude (either via positive redshift evolution or a high local value). The $M_{\text{BH}}-M_{\text{bulge}}$ relation remains the most influential component in GWB amplitude calculations. While an alternative GSMF offers an interesting solution, the GSMF has more robust observational constraints than the $M_{\text{BH}}-M_{\text{bulge}}$ relation outside the local universe. Moreover, the GWB is most directly a probe of SMBH properties and so any inference about the GSMF is a secondary calculation. We therefore conclude that a SMBH-first growth model provides the best fits to the GWB while maintaining a high degree of consistency with EM-based observational constraints.

Future work will investigate the effects of an evolving intrinsic scatter in the $M_{\text{BH}}-M_{\text{bulge}}$ relation. It will also be important to test different evolutionary models using upcoming PTA data releases which will have higher signal-to-noise to better differentiate between models.

ACKNOWLEDGMENTS

The authors would additionally like to thank Joel Leja for insightful discussions which aided and improved the interpretation of this work.

L.B. acknowledges support from the National Science Foundation under award AST-2307171 and from the National Aeronautics and Space Administration under award 80NSSC22K0808. P.R.B. is supported by the Science and Technology Facilities Council, grant number ST/W000946/1. S.B. gratefully acknowledges the support of a Sloan Fellowship, and the support of NSF under award #1815664. The work of R.B., R.C., X.S., J.T., and D.W. is partly supported by the George and Hannah Bolinger Memorial Fund in the College of Science at Oregon State University. M.C., P.P., and S.R.T. acknowledge support from NSF AST-2007993. M.C. was supported by the Vanderbilt Initiative in Data Intensive Astrophysics (VIDA) Fellowship. Support for this work was provided by the NSF through the Grote Reber Fellowship Program administered by Associated Universities, Inc./National Radio Astronomy Observatory. Pulsar research at UBC is supported by an NSERC Discovery Grant and by CIFAR. K.C. is supported by a UBC Four Year Fellowship (6456). M.E.D. acknowledges support from the Naval Research Laboratory by NASA under contract S-15633Y. T.D. and M.T.L. received support by an NSF Astronomy and Astrophysics Grant (AAG) award number 2009468 during this work. E.C.F. is supported by NASA under award number 80GSFC24M0006. G.E.F., S.C.S., and S.J.V. are supported by NSF award PHY-2011772. K.A.G. and S.R.T. acknowledge support from an NSF CAREER award #2146016. A.D.J. and M.V. acknowledge support from the Caltech and Jet Propulsion Laboratory President’s and Director’s Research and Development Fund. A.D.J. acknowledges support from the Sloan Foundation. N.La. acknowledges the support from Larry W. Martin and Joyce B. O’Neill Endowed Fellowship in the College of Science at Oregon State University. Part of this research was carried out at the Jet Propulsion Laboratory, California Institute of Technology, under a contract with the National Aeronautics and Space Administration (80NM0018D0004). D.R.L. and M.A.M. are supported by NSF #1458952. M.A.M. is supported by NSF #2009425. C.M.F.M. was supported in part by

the National Science Foundation under Grants No. NSF PHY-1748958 and AST-2106552. A.Mi. is supported by the Deutsche Forschungsgemeinschaft under Germany’s Excellence Strategy - EXC 2121 Quantum Universe - 390833306. The Dunlap Institute is funded by an endowment established by the David Dunlap family and the University of Toronto. K.D.O. was supported in part by NSF Grant No. 2207267. T.T.P. acknowledges support from the Extragalactic Astrophysics Research Group at Eötvös Loránd University, funded by the Eötvös Loránd Research Network (ELKH), which was used during the development of this research. H.A.R. is supported by NSF Partnerships for Research and Education in Physics (PREP) award No. 2216793. S.M.R. and I.H.S. are CIFAR Fellows. Portions of this work performed at NRL were supported by ONR 6.1 basic research funding. J.D.R. also acknowledges support from start-up funds from Texas Tech University. J.S. is supported by an NSF Astronomy and Astrophysics Postdoctoral Fellowship under award AST-2202388, and acknowledges previous support by the NSF under award 1847938. O.Y. is supported by the National Science Foundation Graduate Research Fellowship under Grant No. DGE-2139292.

Anishinaabeg gaa bi dinokiiwaad temigad manda Michigan Kichi Kinoomaagegamig. Mdaaswi nshwaaswaak shi mdaaswi shi niizhawaaswi gii-sababoonagak, Ojibweg, Odawaag, minwaa Bodwe’aadamiig wiiba gii-miigwenaa’aa maamoonjini-ibina Kichi Kinoomaagegamigoong wi pii-gaa aanjibi-igaadeg Kichi-Naakonigewinning, debendang manda aki, mampii Niisaajiwan, gewiinwaa niijaansiwaan ji kinoomaagaazinid. Daapanaming ninda kidwinan, megwaa minwaa gaa bi aankoosejig zhinda akiing minwaa gii-miigwewaad Kichi-Kinoomaagegamigoong aanjidaapinanigaade minwaa mshkowenjigaade.

The University of Michigan is located on the traditional territory of the Anishinaabe people. In 1817, the Ojibwe, Odawa, and Bodewadami Nations made the largest single land transfer to the University of Michigan. This was offered ceremonially as a gift through the Treaty at the Foot of the Rapids so that their children could be educated. Through these words of acknowledgment, their contemporary and ancestral ties to the land and their contributions to the University are renewed and reaffirmed.

AUTHOR CONTRIBUTIONS

C.M. was the primary lead for the formal analysis and investigation of this project. C.M. led the writing and editing of this manuscript and produced all figures and models. C.M. K.G. were responsible for the conceptualization and supervision of this work. C.M. and L.Z.K. developed and adapted the software and methodology applied here. K.G. L.Z.K. J.S. and L.B. provided useful feedback and comments as well as aided in scientific interpretation of the results. Additional NANOGrav members are listed in alphabetical order, each contributed toward the collaboration-wide endeavor of pulsar timing which culminated in evidence for the GWB. The work presented in this paper benefits from data collected and analyzed in the course of this search and would not be possible without this large-scale coordination.

Software: Astropy ([Astropy Collaboration et al. 2013](#)) – SciPy ([P. Virtanen et al. 2020](#)) – NumPy ([C. R. Harris et al. 2020](#)) – Matplotlib ([J. D. Hunter 2007](#)) – kalepy ([L. Z. Kelley 2023](#)) – holodeck ([G. Agazie et al. 2023b](#)), cefyl ([W. G. Lamb et al. 2023](#))

APPENDIX

A. GSMF EVOLUTION PARAMETERS AND SCALING RELATION CHOICE

In this section, we describe the form of evolution we assume for the GSMF used in LM11ne and LM11ev. We additionally explore the effects of alternative GSMFs not presented in the main text and briefly investigate the implications for the GWB and high- z galaxy population. The different GSMFs and corresponding GWB spectra are shown in Figure 9. We also describe the effect of $M_{\text{BH}}-M_{\text{bulge}}$ version on the predicted GWB spectrum at the end of this section and in Figure 10.

The GSMF measured by [E. R. Liepold & C.-P. Ma \(2024\)](#) uses only $z = 0$ galaxies and so they do not provide an explicit evolutionary form for the GSMF at higher redshift. For use in our analysis, we construct and test several models that bracket the plausible rates of GSMF evolution. A strongly evolving GSMF is predicted for $0 < z < 1$ (e.g., [G. De Lucia et al. 2007](#)) though observations often show a lack of evolution in this redshift range (e.g., [J. Moustakas et al. 2013](#); [K. Bundy et al. 2017](#); [J. Leja et al. 2020](#)). The [E. R. Liepold & C.-P. Ma \(2024\)](#) GSMF offers observational support for this predicted evolution. The GSMF due to [J. Leja et al. \(2020\)](#) does not show significant evolution for

Evolution Type	$\phi_{*,1,0}$	$\phi_{*,1,1}$	$\phi_{*,1,2}$	$\phi_{*,2,0}$	$\phi_{*,2,1}$	$\phi_{*,2,2}$	$M_{c,0}$	$M_{c,1}$	$M_{c,2}$	α_1	α_2
Strong	-4.85	-0.33	-0.137	-2.85	-0.460	0.057	11.33	0.0155	-0.0413	0.92	-1.38
Moderate	-4.85	-0.26	-0.110	-2.85	-0.370	0.050	11.33	0.0200	-0.0300	0.92	-1.38
Weak	-4.85	-0.33	-0.137	-2.85	-0.460	0.057	11.33	0.1550	-0.0413	0.92	-1.38

Table 3. The explicit evolution parameters for the strongly evolving version of the [E. R. Liepold & C.-P. Ma \(2024\)](#) GSMF. Values under parameters with subscript 0 are equivalent to the combined M_* local values presented in [E. R. Liepold & C.-P. Ma \(2024\)](#). The other columns are the evolutionary parameters (see equations 3–5).

$0 < z < 1$ which, according to [E. R. Liepold & C.-P. Ma \(2024\)](#) could be due to observational biases in the local universe. Large cosmological surveys do not have the appropriate local volume to catch the most massive galaxies and so the [E. R. Liepold & C.-P. Ma \(2024\)](#) GSMF offers to complete the picture for the local high-mass GSMF. The [J. Leja et al. \(2020\)](#) GSMF is consistent with many other studies and theory for $1 < z < 3$, and there is no strong foundation to believe that the GSMF in this redshift range is invalid. We can assume that the [J. Leja et al. \(2020\)](#) GSMF is complete for $z \gtrsim 1$ and can therefore find an approximate evolution that matches the local [E. R. Liepold & C.-P. Ma \(2024\)](#) GSMF and also the [J. Leja et al. \(2020\)](#) for $z \gtrsim 1$.

Starting with the explicit $z = 0$ GSMF from [E. R. Liepold & C.-P. Ma \(2024\)](#) and assuming a similar functional form to that in [J. Leja et al. \(2020\)](#), we tested three different forms of evolution represented by the shaded regions in Figure 9: (i) Weakly evolving (green): producing a GWB amplitude similar to that in [E. R. Liepold & C.-P. Ma \(2024\)](#), (ii) Moderately evolving (orange), and (iii) Strongly evolving (blue): Designed to match the high-mass end of the [J. Leja et al. \(2020\)](#) GSMF by a redshift of $z \gtrsim 1$, all parameters for these models are given in Table 3.

We believe the strongly evolving model to be the most faithful to the observational constraints from both [E. R. Liepold & C.-P. Ma \(2024\)](#) and [J. Leja et al. \(2020\)](#) hence this is the model we use for our analysis. The strongly evolving GSMF produces the lowest number densities at higher redshift compared to the other two evolutionary forms. The parameters for the strongly evolving GSMF were chosen such that the number density of massive galaxies is roughly similar to that of [J. Leja et al. \(2020\)](#) by redshift $z \sim 1$. This option bridges the gap between the local GSMF from [E. R. Liepold & C.-P. Ma \(2024\)](#) while maintaining consistency with [J. Leja et al. \(2020\)](#) and therefore represents the solution that is in agreement with both observational constraints. This is the model we use in LM11ne and LM11ev, the results of which are discussed in the main text in section 3.1.2.

The weakly evolving GSMF produces the highest GWB amplitude and is nearly consistent with the PTA data. In fact, only minor changes to, e.g., the hardening timescales would be needed to match the PTA data. This option represents the number density of galaxies that best reproduces the GWB starting from the local GSMF in [E. R. Liepold & C.-P. Ma \(2024\)](#) and without significantly changing any other assumptions in our model. We only provide this approximate form and do not perform any fits because this GSMF is unrealistic and only used for demonstration purposes.

The moderately evolving GSMF represents a sort of “compromise” between the other two extremes. Interestingly, the posterior GSMF from LM11ne is very similar to this toy model we present here. The change in number density across $0 < z < 3$ is actually greater than in [J. Leja et al. \(2020\)](#), though it is positively offset at every redshift compared to their GSMF. This GSMF could be a realistic representation of the high- z population, but would suggest that we are vastly underestimating galaxy stellar masses at these redshifts (e.g., via an incorrect initial mass function) or that cosmological surveys are largely incomplete (by a factor of 10 or more) in this regime. At this time we cannot evaluate the feasibility of this GSMF though, as emphasized earlier in section 4, the inferences made for the GSMF from the GWB are to be treated with a high degree of caution.

In Figure 10 we demonstrate the impact of scaling relation choice on the GWB spectrum. The version of the scaling relation from [J. Kormendy & L. C. Ho \(2013\)](#) generally produces bigger SMBHs (and therefore higher GWB amplitudes) than other options (see, e.g., [J. Simon 2023](#)). [E. R. Liepold & C.-P. Ma \(2024\)](#) use the [N. J. McConnell & C.-P. Ma \(2013\)](#) version of the $M_{\text{BH}}-M_{\text{bulge}}$ relation, which generally produces lower GWB amplitudes compared to [J. Kormendy & L. C. Ho \(2013\)](#). We additionally show the GWB spectrum using the scaling relation from [F. Shankar et al. \(2016\)](#).

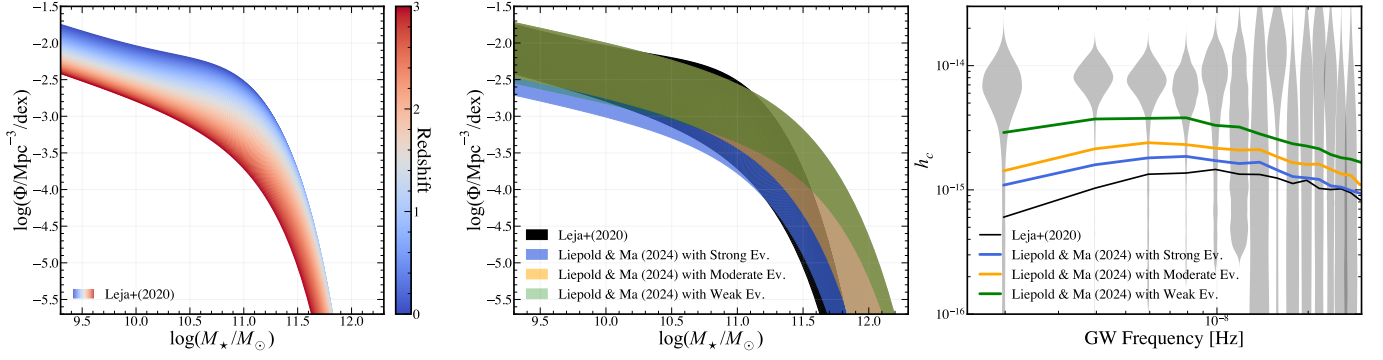


Figure 9. A comparison between the *J. Leja et al. (2020)* GSMF (left red/blue and middle black) and our evolving versions of the *E. R. Liepold & C.-P. Ma (2024)* GSMF (middle blue, orange, and green). The right panel shows the corresponding fiducial GWB spectra corresponding to each of these models. The GSMFs in the right and middle panels are all defined for $0 < z < 3$. The strongly evolving GSMF (blue) we consider is only negligibly different to that in *J. Leja et al. (2020)* for $M_* \geq 10^{11} M_\odot$ (which corresponds to the SMBH masses contributing to the GWB the most) for $z \geq 1$. In this case we only see a minimal increase in amplitude to the GWB spectrum. In fact, even the weakly evolving GSMF (green) falls just short of the GWB data indicating that, a nearly non-evolving GSMF would be needed to match the GWB without changing other model parameters. For all GWB spectra shown here we use the *J. Kormendy & L. C. Ho (2013)* $M_{\text{BH}}-M_{\text{bulge}}$ relation.

This comparison demonstrates that, wherever our spectra fall short of the GWB data, using a relation with a lower amplitude would only exacerbate this problem. This also has implications for our choices for the evolution we approximate for the *E. R. Liepold & C.-P. Ma (2024)* GSMF. The moderately evolving GSMF would produce a much lower GWB amplitude if we use the *N. J. McConnell & C.-P. Ma (2013)* or *F. Shankar et al. (2016)* relations and so either the evolution would need to be more similar to that of the weakly evolving GSMF or a higher-amplitude $M_{\text{BH}}-M_{\text{bulge}}$ relation is needed.

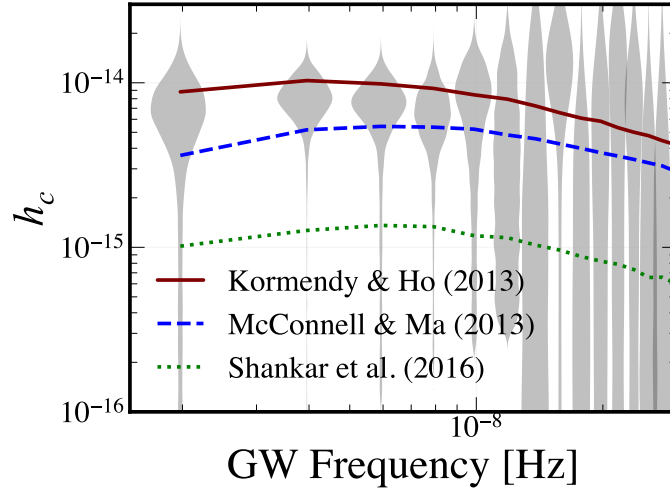


Figure 10. This figure demonstrates how the choice in scaling relation between *J. Kormendy & L. C. Ho (2013)*, *N. J. McConnell & C.-P. Ma (2013)*, and *F. Shankar et al. (2016)* affects the GWB spectrum. Because the *J. Kormendy & L. C. Ho (2013)* relation has a higher amplitude and steeper slope than *N. J. McConnell & C.-P. Ma (2013)* and *F. Shankar et al. (2016)*, the spectrum is broadly higher in amplitude with the biggest increase at the lower-frequency end.

B. CORNER PLOTS

The full corner plots for each of our 8 models. Note that the variables pertaining to galaxy merger rates include “GMR” in the subscript to distinguish from other parameters which use similar variables. For the parameters in the model not detailed in this paper we refer the reader to *G. Agazie et al. (2023b)* (and references therein) for a complete

discussion. In each corner plot, the blue histograms / contours represent the posterior distributions. The priors are shown by the gray histograms.

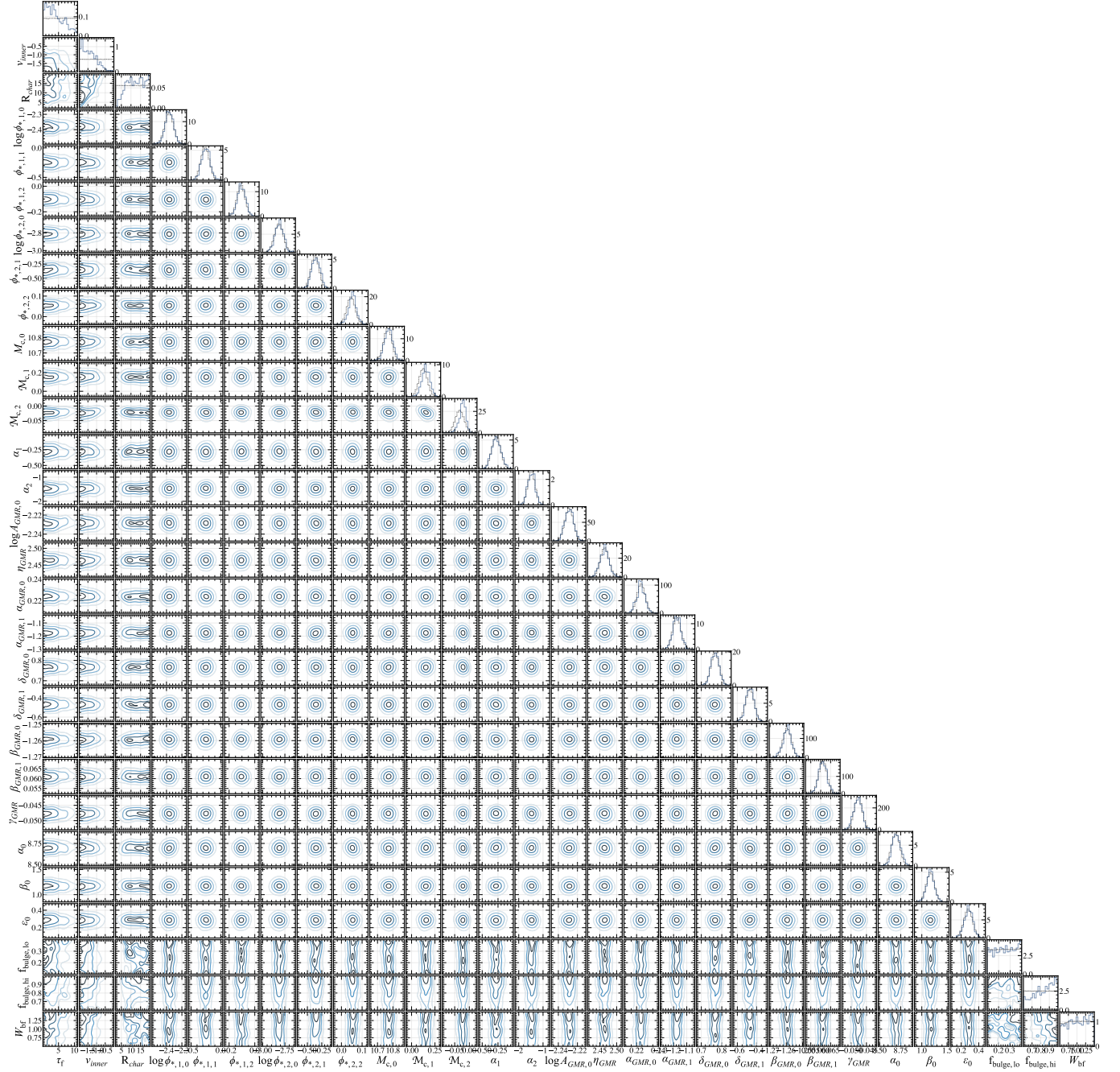


Figure 11. Complete corner plot for Le11ne.

C. RELIABILITY OF METHODS

Here we demonstrate that our “direct-likelihood” method reproduces the Gaussian process-interpolated MCMC-like methods of G. Agazie et al. (2023b). In Figure 19 we show a comparison between the posterior distributions from G. Agazie et al. (2023a) compared to our results when using the same prior model set up. We see that the two methods return negligibly different posterior distributions. The method we use in this work is also discussed in more depth in Appendix C of G. Agazie et al. (2023b).

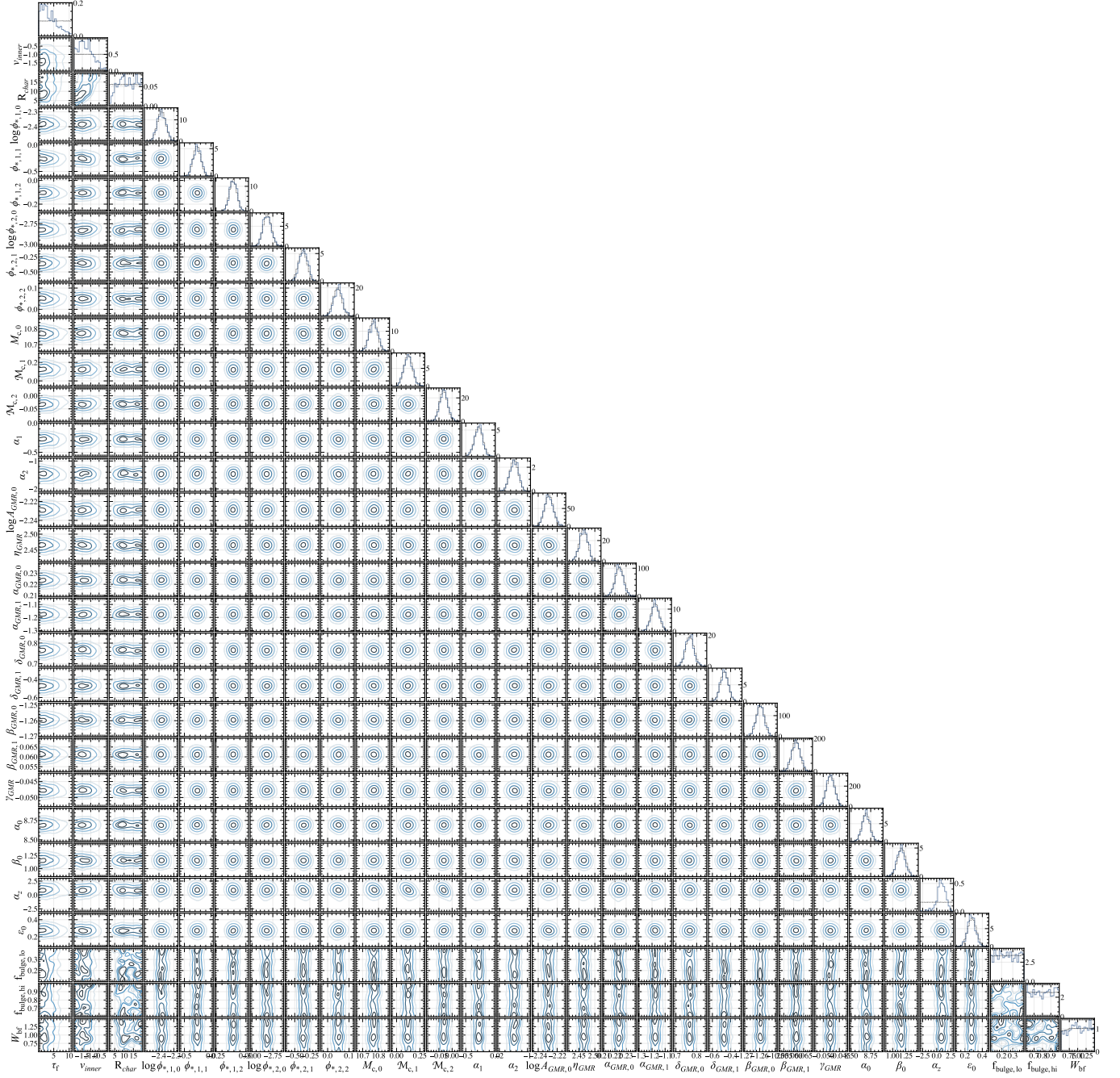


Figure 12. Complete corner plot for Le11ev.

In this work we discovered a minor limitation of the direct-likelihood method which impacted the Le00ne model. It is more difficult for the posterior distributions to deviate from the priors because extreme values (e.g. more than 3σ above or below the prior median) have a low chance of being randomly sampled, regardless of how well that value may describe the data. We see this limitation in our model with the lowest number of sampled parameters, Le00ne. The best-fit GWB spectrum from this model returned a notably low log-likelihood compared to the other models and produces a worse overall fit (see Figures 3 and 6). We can see, from Le03ev and Le00ev, that a value of $\alpha(z) > 9.0$ is needed to reproduce the GWB amplitude without increasing galaxy number density. If the $M_{\text{BH}}-M_{\text{bulge}}$ relation is not allowed to evolve, the prior for α_0 would need to be sampled at a value $\gtrsim 6\sigma$ away from the prior mean (assuming a normal distribution where $\alpha_0 = 8.69 \pm 0.055$), and therefore extremely unlikely / impossible to be sampled. Without

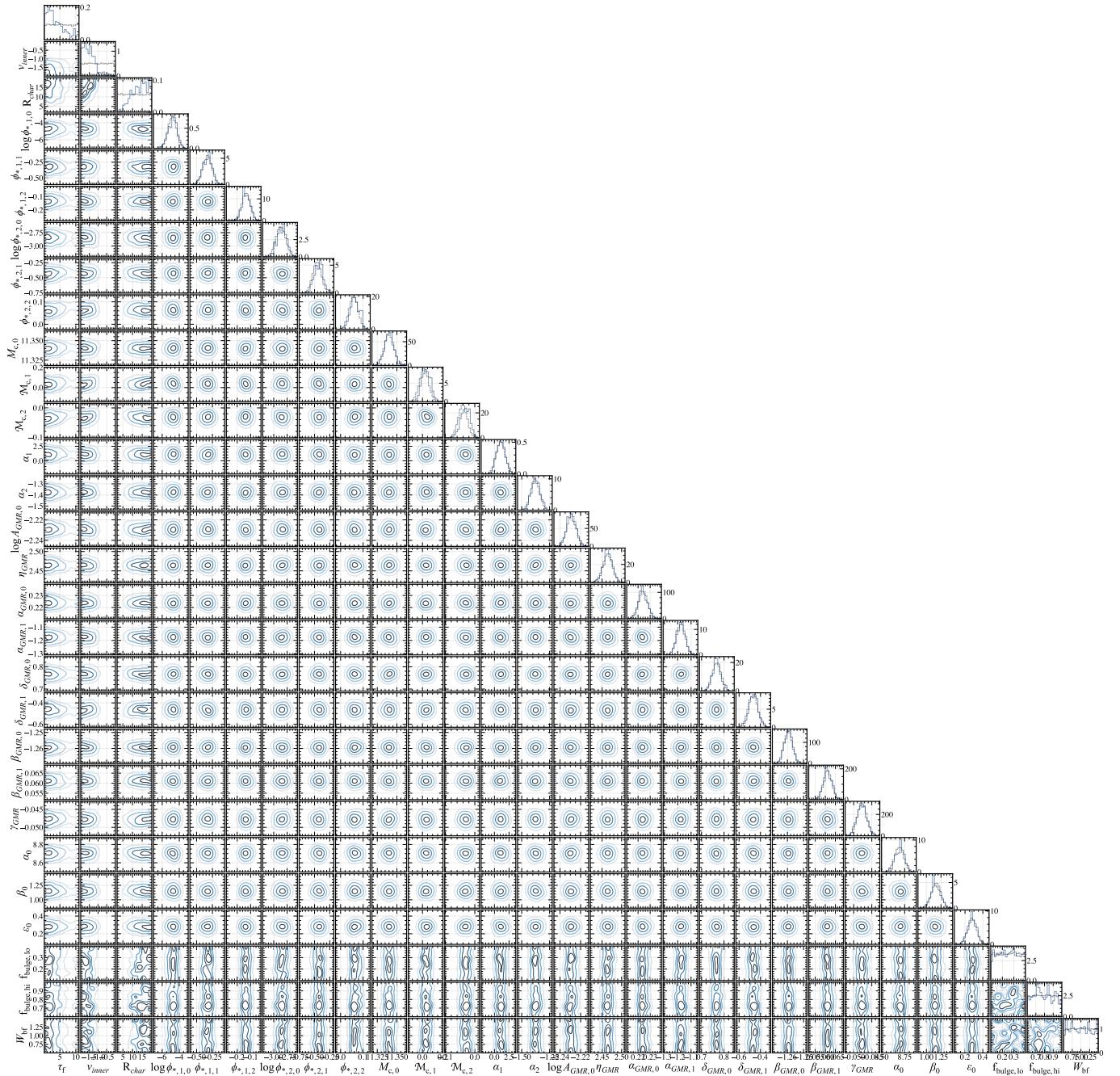


Figure 13. Complete corner plot for LM11ne.

interpolating, any value that is not sampled simply does not have a corresponding GWB spectrum and the best-fit parameters may therefore not describe the data. This effect can be mitigated by choice of priors, but prior choice has its own impact on models and so future studies should consider the impact of this effect when using this method.

REFERENCES

Agazie, G., Anumalapudi, A., Archibald, A. M., et al.

Agazie, G., Anumalapudi, A., Archibald, A. M., et al.

2023a, ApJL, 951, L8, doi: [10.3847/2041-8213/acdac6](https://doi.org/10.3847/2041-8213/acdac6)

2023b, ApJL, 952, L37, doi: [10.3847/2041-8213/ace18b](https://doi.org/10.3847/2041-8213/ace18b)

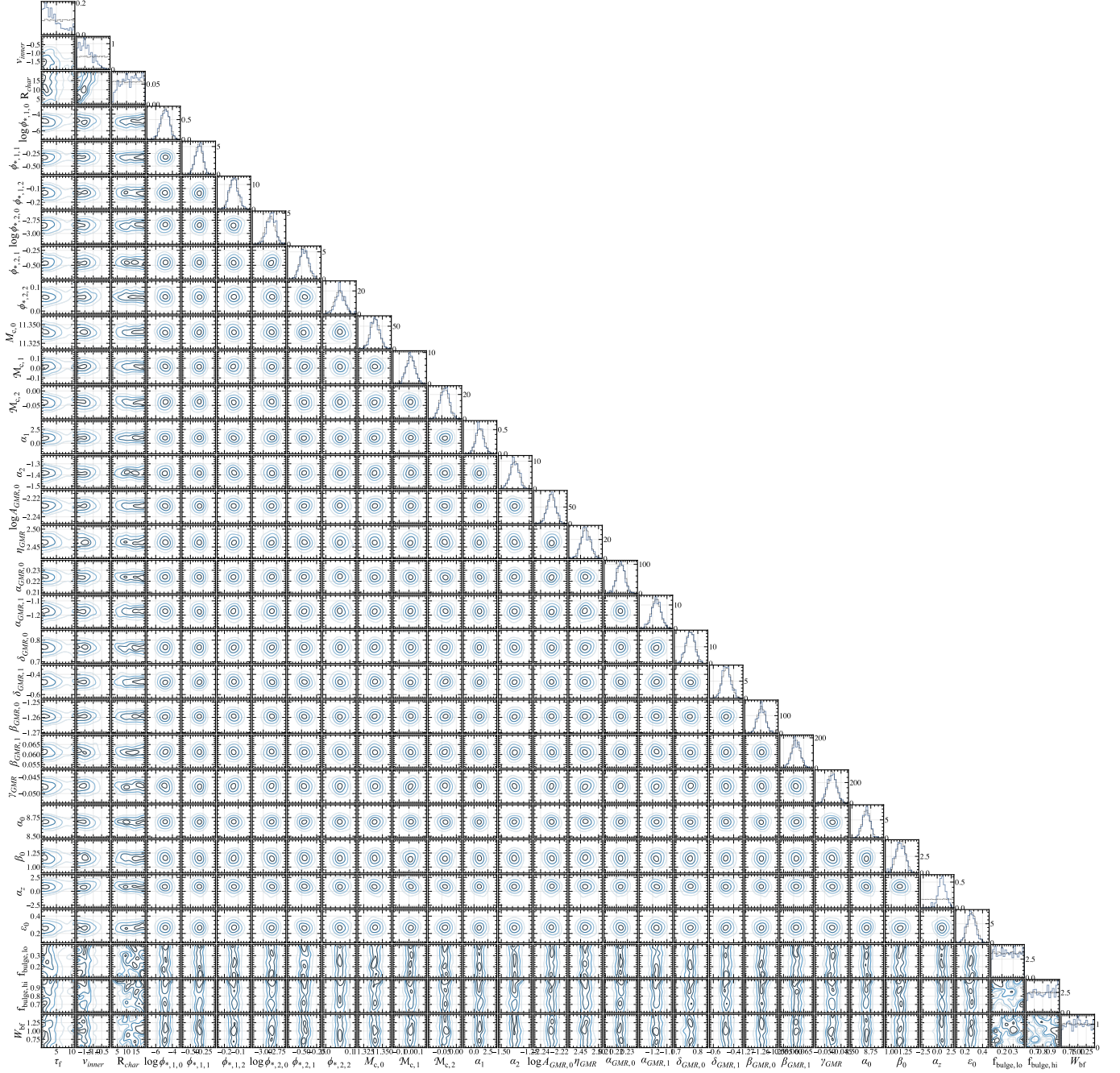


Figure 14. Complete corner plot for LM11ev.

Astropy Collaboration, Robitaille, T. P., Tollerud, E. J., et al. 2013, *A&A*, 558, A33,

doi: [10.1051/0004-6361/201322068](https://doi.org/10.1051/0004-6361/201322068)

Barausse, E., Shankar, F., Bernardi, M., Dubois, Y., & Sheth, R. K. 2017, *MNRAS*, 468, 4782,

doi: [10.1093/mnras/stx799](https://doi.org/10.1093/mnras/stx799)

Begelman, M. C., Blandford, R. D., & Rees, M. J. 1980, *Nature*, 287, 307, doi: [10.1038/287307a0](https://doi.org/10.1038/287307a0)

Behroozi, P., Conroy, C., Wechsler, R. H., et al. 2020, *MNRAS*, 499, 5702, doi: [10.1093/mnras/staa3164](https://doi.org/10.1093/mnras/staa3164)

Bennert, V. N., Auger, M. W., Treu, T., Woo, J.-H., & Malkan, M. A. 2011, *ApJ*, 742, 107,

doi: [10.1088/0004-637X/742/2/107](https://doi.org/10.1088/0004-637X/742/2/107)

Bernardi, M., Meert, A., Sheth, R. K., et al. 2013, *MNRAS*, 436, 697, doi: [10.1093/mnras/stt1607](https://doi.org/10.1093/mnras/stt1607)

Bogdán, Á., Goulding, A. D., Natarajan, P., et al. 2024, *Nature Astronomy*, 8, 126,

doi: [10.1038/s41550-023-02111-9](https://doi.org/10.1038/s41550-023-02111-9)

Bundy, K., Leauthaud, A., Saito, S., et al. 2017, *ApJ*, 851, 34, doi: [10.3847/1538-4357/aa9896](https://doi.org/10.3847/1538-4357/aa9896)

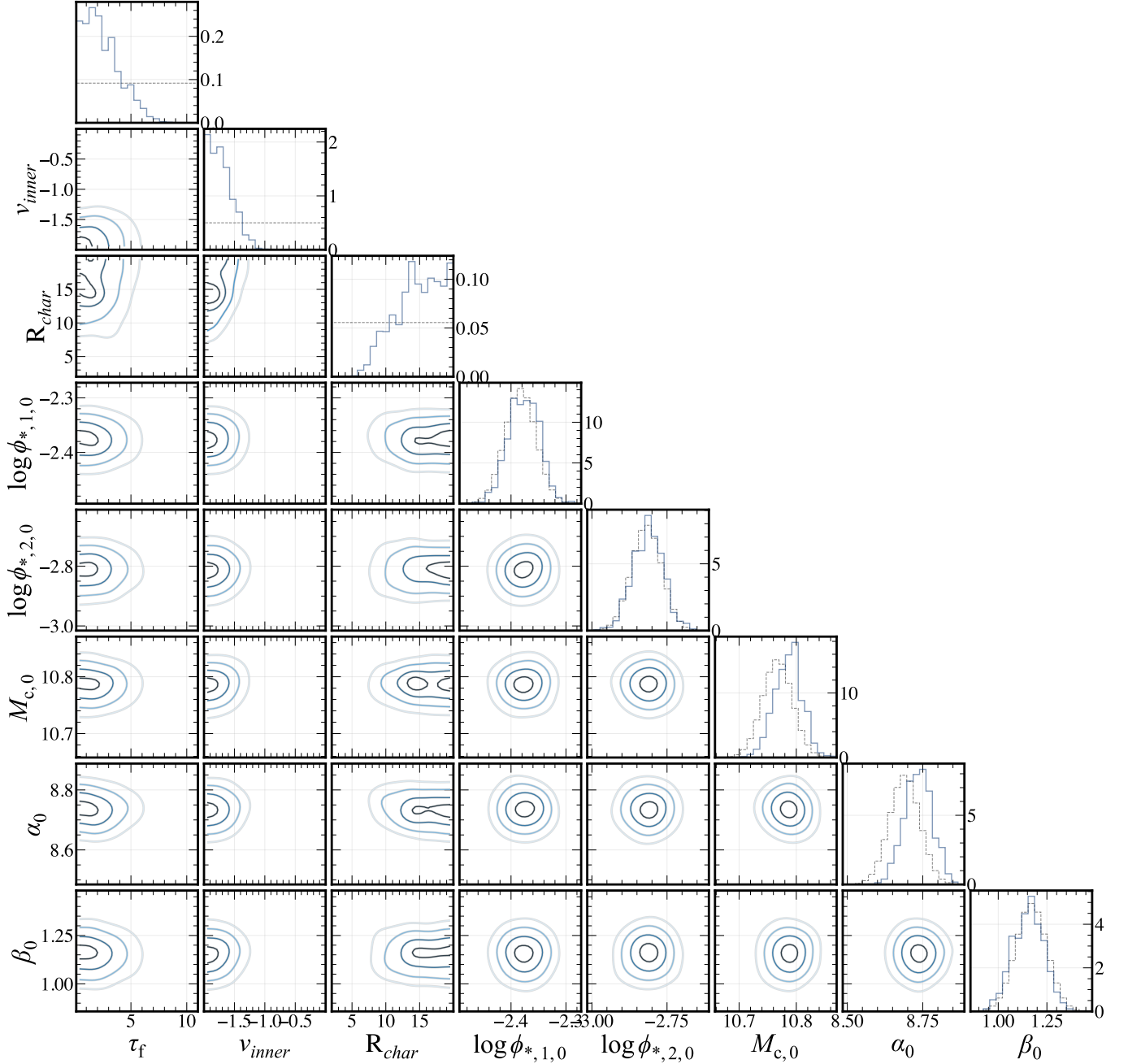


Figure 15. Complete corner plot for Le03ne.

Burke-Spolaor, S., Taylor, S. R., Charisi, M., et al. 2019, *A&A Rv*, 27, 5, doi: [10.1007/s00159-019-0115-7](https://doi.org/10.1007/s00159-019-0115-7)

Cattaneo, A., Blaizot, J., Devriendt, J., & Guiderdoni, B. 2005, *MNRAS*, 364, 407, doi: [10.1111/j.1365-2966.2005.09608.x](https://doi.org/10.1111/j.1365-2966.2005.09608.x)

Chen, S., Sesana, A., & Conselice, C. J. 2019a, *MNRAS*, 488, 401, doi: [10.1093/mnras/stz1722](https://doi.org/10.1093/mnras/stz1722)

Chen, S., Sesana, A., & Conselice, C. J. 2019b, *MNRAS*, 488, 401, doi: [10.1093/mnras/stz1722](https://doi.org/10.1093/mnras/stz1722)

Chen, Y., Yu, Q., & Lu, Y. 2020, *ApJ*, 897, 86, doi: [10.3847/1538-4357/ab9594](https://doi.org/10.3847/1538-4357/ab9594)

Chen, Y., Yu, Q., & Lu, Y. 2024, *ApJ*, 974, 261, doi: [10.3847/1538-4357/ad7582](https://doi.org/10.3847/1538-4357/ad7582)

Cisternas, M., Jahnke, K., Bongiorno, A., et al. 2011, *ApJL*, 741, L11, doi: [10.1088/2041-8205/741/1/L11](https://doi.org/10.1088/2041-8205/741/1/L11)

Cloonan, A. P., Khullar, G., Napier, K. A., et al. 2024, arXiv e-prints, arXiv:2408.03379, doi: [10.48550/arXiv.2408.03379](https://doi.org/10.48550/arXiv.2408.03379)

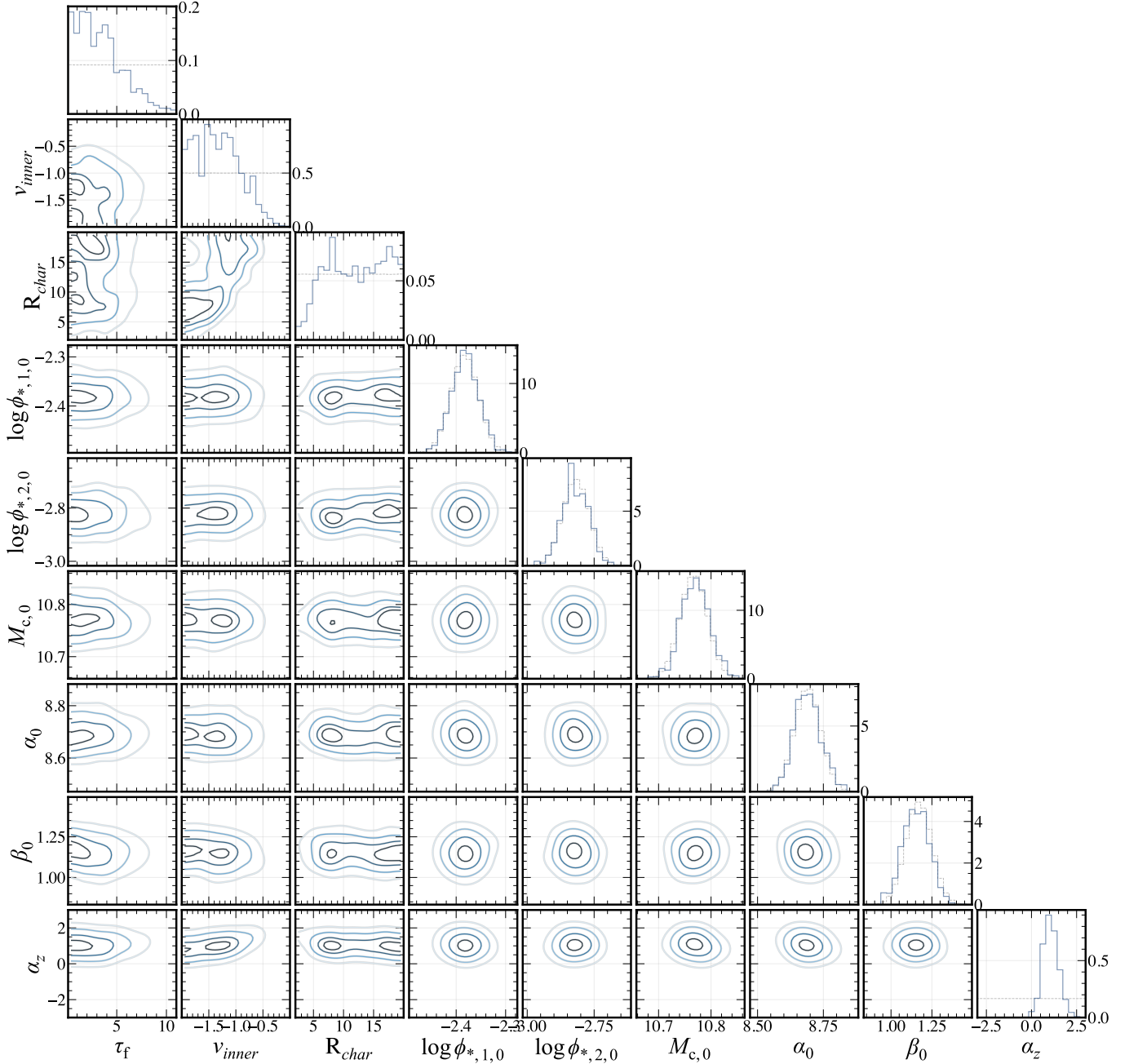


Figure 16. Complete corner plot for Le11ev.

Cohn, J. H., Durodola, E., Casey, Q. O., Lambrides, E., & Hickox, R. C. 2025, arXiv e-prints, arXiv:2504.00172, doi: [10.48550/arXiv.2504.00172](https://doi.org/10.48550/arXiv.2504.00172)

Croton, D. J. 2006, MNRAS, 369, 1808, doi: [10.1111/j.1365-2966.2006.10429.x](https://doi.org/10.1111/j.1365-2966.2006.10429.x)

Davidzon, I., Ilbert, O., Laigle, C., et al. 2017, A&A, 605, A70, doi: [10.1051/0004-6361/201730419](https://doi.org/10.1051/0004-6361/201730419)

de Graaff, A., Bezanson, R., Franx, M., et al. 2021, ApJ, 913, 103, doi: [10.3847/1538-4357/abf1e7](https://doi.org/10.3847/1538-4357/abf1e7)

De Lucia, G., Poggianti, B. M., Aragón-Salamanca, A., et al. 2007, MNRAS, 374, 809, doi: [10.1111/j.1365-2966.2006.11199.x](https://doi.org/10.1111/j.1365-2966.2006.11199.x)

Decarli, R., Falomo, R., Treves, A., et al. 2010, MNRAS, 402, 2453, doi: [10.1111/j.1365-2966.2009.16049.x](https://doi.org/10.1111/j.1365-2966.2009.16049.x)

Dickey, J. M. 1971, The Annals of Mathematical Statistics, 42, 204, doi: [10.1214/aoms/1177693507](https://doi.org/10.1214/aoms/1177693507)

Ding, X., Silverman, J., Treu, T., et al. 2020, ApJ, 888, 37, doi: [10.3847/1538-4357/ab5b90](https://doi.org/10.3847/1538-4357/ab5b90)

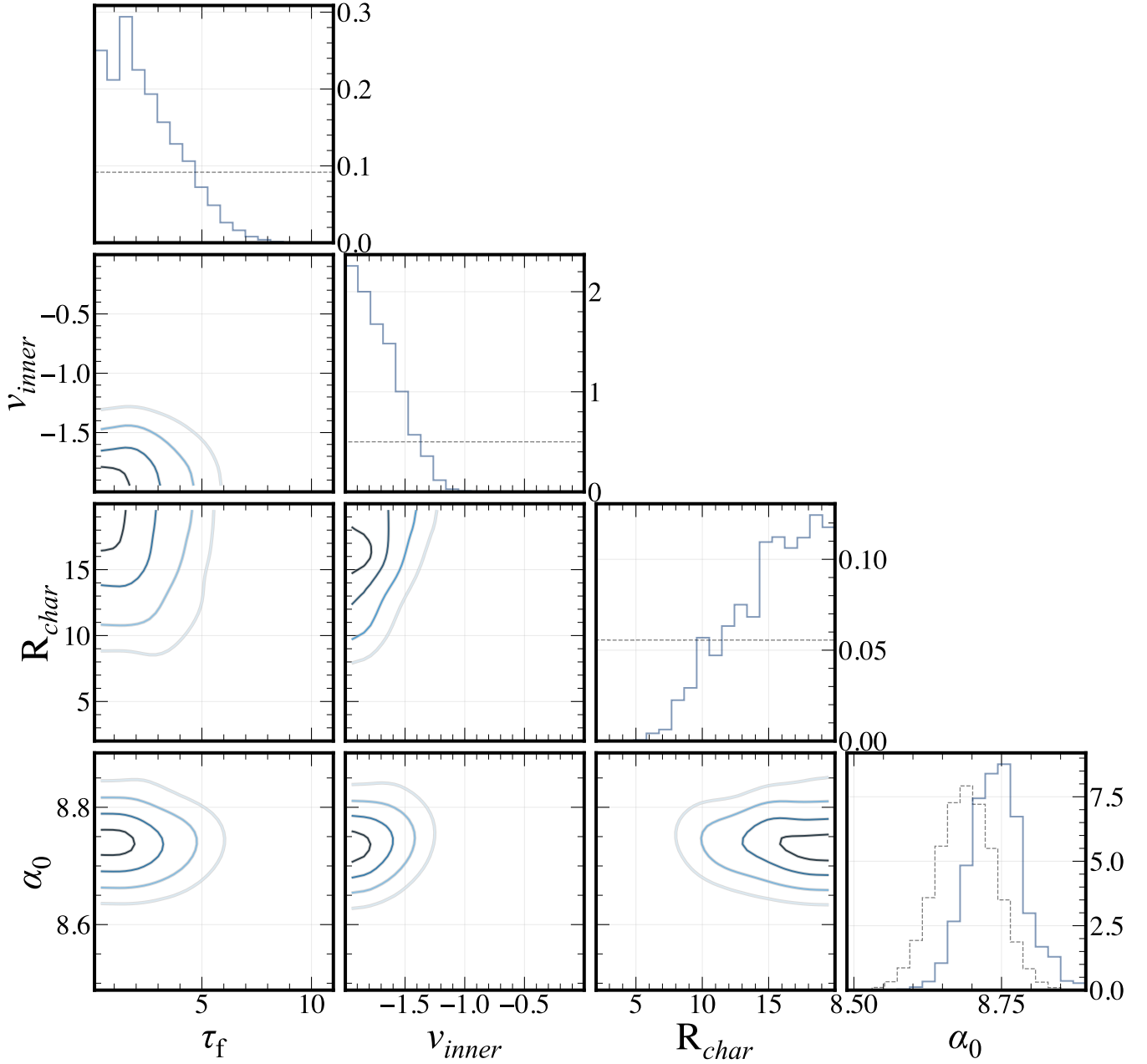


Figure 17. Complete corner plot for Le00ne.

D’Souza, R., Vegetti, S., & Kauffmann, G. 2015, MNRAS, 454, 4027, doi: [10.1093/mnras/stv2234](https://doi.org/10.1093/mnras/stv2234)

EPTA Collaboration, InPTA Collaboration, Antoniadis, J., et al. 2023, A&A, 678, A50, doi: [10.1051/0004-6361/202346844](https://doi.org/10.1051/0004-6361/202346844)

Ferrarese, L., & Merritt, D. 2000, ApJL, 539, L9, doi: [10.1086/312838](https://doi.org/10.1086/312838)

Gardiner, E. C., Kelley, L. Z., Lemke, A.-M., & Mitridate, A. 2023, arXiv e-prints, arXiv:2309.07227, doi: [10.48550/arXiv.2309.07227](https://doi.org/10.48550/arXiv.2309.07227)

Gebhardt, K., Bender, R., Bower, G., et al. 2000, ApJL, 539, L13, doi: [10.1086/312840](https://doi.org/10.1086/312840)

Harikane, Y., Zhang, Y., Nakajima, K., et al. 2023, ApJ, 959, 39, doi: [10.3847/1538-4357/ad029e](https://doi.org/10.3847/1538-4357/ad029e)

Harris, C. R., Millman, K. J., van der Walt, S. J., et al. 2020, Nature, 585, 357, doi: [10.1038/s41586-020-2649-2](https://doi.org/10.1038/s41586-020-2649-2)

Hellings, R. W., & Downs, G. S. 1983, ApJL, 265, L39, doi: [10.1086/183954](https://doi.org/10.1086/183954)

Hirschmann, M., Khochfar, S., Burkert, A., et al. 2010, MNRAS, 407, 1016, doi: [10.1111/j.1365-2966.2010.17006.x](https://doi.org/10.1111/j.1365-2966.2010.17006.x)

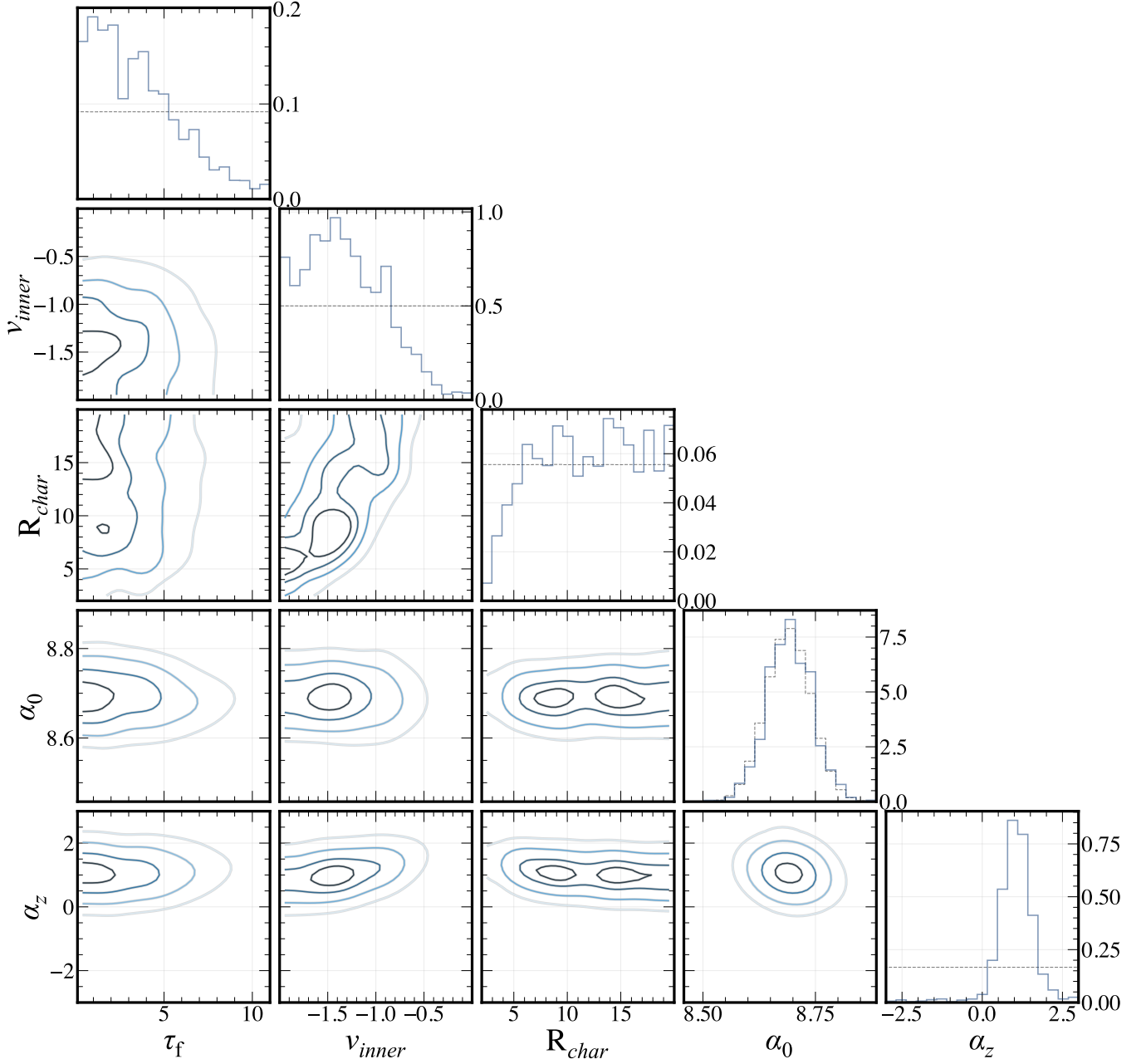


Figure 18. Complete corner plot for Le00ev.

Hopkins, P. F., Hernquist, L., Cox, T. J., Keres, D., & Wuyts, S. 2009, *ApJ*, 691, 1424, doi: [10.1088/0004-637X/691/2/1424](https://doi.org/10.1088/0004-637X/691/2/1424)

Hoshi, A., Yamada, T., Kokubo, M., Matsuoka, Y., & Nagao, T. 2024, *ApJ*, 969, 11, doi: [10.3847/1538-4357/ad414c](https://doi.org/10.3847/1538-4357/ad414c)

Hu, H., Inayoshi, K., Haiman, Z., Ho, L. C., & Ohsuga, K. 2025, arXiv e-prints, arXiv:2503.03870, doi: [10.48550/arXiv.2503.03870](https://doi.org/10.48550/arXiv.2503.03870)

Hunter, J. D. 2007, *Computing in Science & Engineering*, 9, 90, doi: [10.1109/MCSE.2007.55](https://doi.org/10.1109/MCSE.2007.55)

Jahnke, K., & Macciò, A. V. 2011, *ApJ*, 734, 92, doi: [10.1088/0004-637X/734/2/92](https://doi.org/10.1088/0004-637X/734/2/92)

Jahnke, K., Bongiorno, A., Brusa, M., et al. 2009, *ApJL*, 706, L215, doi: [10.1088/0004-637X/706/2/L215](https://doi.org/10.1088/0004-637X/706/2/L215)

Jeon, J., Liu, B., Taylor, A. J., et al. 2025, arXiv e-prints, arXiv:2503.14703, doi: [10.48550/arXiv.2503.14703](https://doi.org/10.48550/arXiv.2503.14703)

Juodžbalis, I., Maiolino, R., Baker, W. M., et al. 2025, arXiv e-prints, arXiv:2504.03551, doi: [10.48550/arXiv.2504.03551](https://doi.org/10.48550/arXiv.2504.03551)

Kelley, L. Z. 2023, *The Journal of Open Source Software*

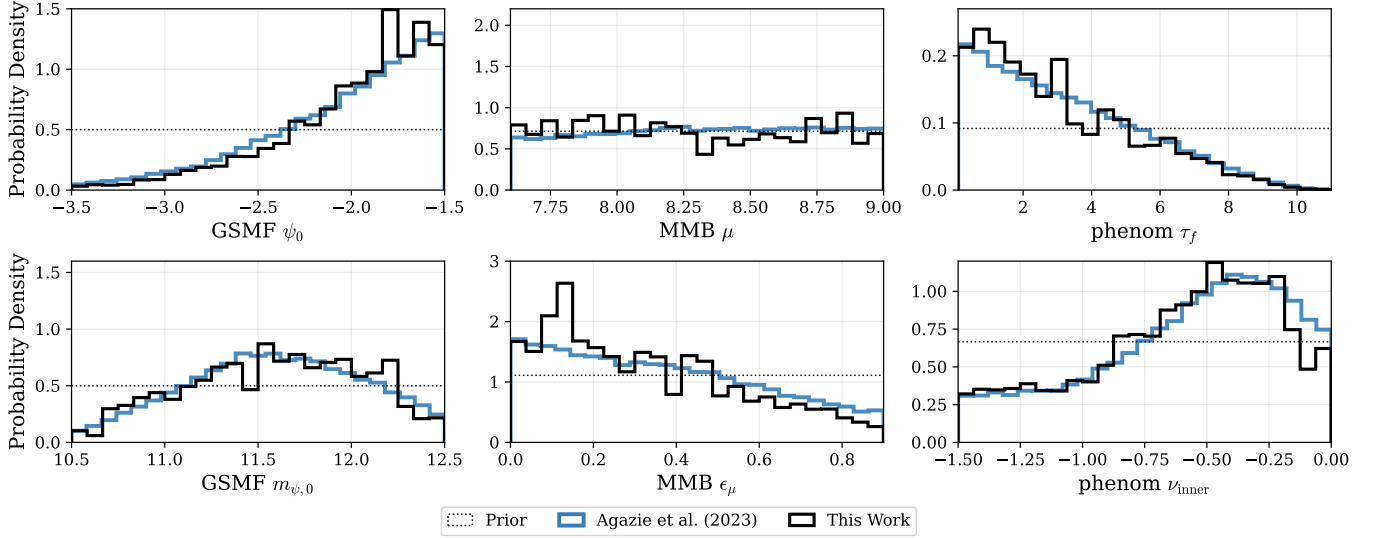


Figure 19. Posterior distributions for the same model set up from G. Agazie et al. (2023b) when using our method (blue) versus theirs (black). We find that our results are in good agreement with theirs when using the same model.

Kormendy, J., & Gebhardt, K. 2001, in American Institute of Physics Conference Series, Vol. 586, 20th Texas Symposium on relativistic astrophysics, ed. J. C. Wheeler & H. Martel (AIP), 363–381, doi: [10.1063/1.1419581](https://doi.org/10.1063/1.1419581)

Kormendy, J., & Ho, L. C. 2013, ARA&A, 51, 511, doi: [10.1146/annurev-astro-082708-101811](https://doi.org/10.1146/annurev-astro-082708-101811)

Kozhikkal, M. M., Chen, S., Theureau, G., Habouzit, M., & Sesana, A. 2024, MNRAS, 531, 1931, doi: [10.1093/mnras/stae1219](https://doi.org/10.1093/mnras/stae1219)

Laal, N., Taylor, S. R., Kelley, L. Z., et al. 2025, ApJ, 982, 55, doi: [10.3847/1538-4357/adb4ef](https://doi.org/10.3847/1538-4357/adb4ef)

Laigle, C., McCracken, H. J., Ilbert, O., et al. 2016, ApJS, 224, 24, doi: [10.3847/0067-0049/224/2/24](https://doi.org/10.3847/0067-0049/224/2/24)

Lamb, W. G., Taylor, S. R., & van Haasteren, R. 2023, Physical Review D, 108, 103019

Lauer, T. R., Tremaine, S., Richstone, D., & Faber, S. M. 2007, ApJ, 670, 249, doi: [10.1086/522083](https://doi.org/10.1086/522083)

Leja, J., Speagle, J. S., Johnson, B. D., et al. 2020, ApJ, 893, 111, doi: [10.3847/1538-4357/ab7e27](https://doi.org/10.3847/1538-4357/ab7e27)

Li, J., Shen, Y., & Zhuang, M.-Y. 2025, arXiv e-prints, arXiv:2502.05048, doi: [10.48550/arXiv.2502.05048](https://doi.org/10.48550/arXiv.2502.05048)

Li, J., Silverman, J. D., Ding, X., et al. 2021, ApJ, 922, 142, doi: [10.3847/1538-4357/ac2301](https://doi.org/10.3847/1538-4357/ac2301)

Liepold, E. R., & Ma, C.-P. 2024, ApJL, 971, L29, doi: [10.3847/2041-8213/ad66b8](https://doi.org/10.3847/2041-8213/ad66b8)

Ma, C.-P., Greene, J. E., McConnell, N., et al. 2014, ApJ, 795, 158, doi: [10.1088/0004-637X/795/2/158](https://doi.org/10.1088/0004-637X/795/2/158)

Maiolino, R., Scholtz, J., Curtis-Lake, E., et al. 2024a, A&A, 691, A145, doi: [10.1051/0004-6361/202347640](https://doi.org/10.1051/0004-6361/202347640)

Maiolino, R., Scholtz, J., Witstok, J., et al. 2024b, Nature, 627, 59, doi: [10.1038/s41586-024-07052-5](https://doi.org/10.1038/s41586-024-07052-5)

Matt, C., Gültekin, K., & Simon, J. 2023, MNRAS, 524, 4403, doi: [10.1093/mnras/stad2146](https://doi.org/10.1093/mnras/stad2146)

Matthee, J., Naidu, R. P., Brammer, G., et al. 2024, ApJ, 963, 129, doi: [10.3847/1538-4357/ad2345](https://doi.org/10.3847/1538-4357/ad2345)

McConnell, N. J., & Ma, C.-P. 2013, ApJ, 764, 184, doi: [10.1088/0004-637X/764/2/184](https://doi.org/10.1088/0004-637X/764/2/184)

McLeod, D. J., McLure, R. J., Dunlop, J. S., et al. 2021, Monthly Notices of the Royal Astronomical Society, 503, 4413, doi: [10.1093/mnras/stab731](https://doi.org/10.1093/mnras/stab731)

Merloni, A., Bongiorno, A., Bolzonella, M., et al. 2010, ApJ, 708, 137, doi: [10.1088/0004-637X/708/1/137](https://doi.org/10.1088/0004-637X/708/1/137)

Milosavljević, M., & Merritt, D. 2001, ApJ, 563, 34, doi: [10.1086/323830](https://doi.org/10.1086/323830)

Moustakas, J., Coil, A. L., Aird, J., et al. 2013, ApJ, 767, 50, doi: [10.1088/0004-637X/767/1/50](https://doi.org/10.1088/0004-637X/767/1/50)

Muzzin, A., Marchesini, D., Stefanon, M., et al. 2013, ApJ, 777, 18, doi: [10.1088/0004-637X/777/1/18](https://doi.org/10.1088/0004-637X/777/1/18)

Napolitano, L., Castellano, M., Pentericci, L., et al. 2024, arXiv e-prints, arXiv:2410.18763, doi: [10.48550/arXiv.2410.18763](https://doi.org/10.48550/arXiv.2410.18763)

Pacucci, F., & Loeb, A. 2024, ApJ, 964, 154, doi: [10.3847/1538-4357/ad3044](https://doi.org/10.3847/1538-4357/ad3044)

Pacucci, F., Nguyen, B., Carniani, S., Maiolino, R., & Fan, X. 2023, ApJL, 957, L3, doi: [10.3847/2041-8213/ad0158](https://doi.org/10.3847/2041-8213/ad0158)

Peng, C. Y. 2007, ApJ, 671, 1098, doi: [10.1086/522774](https://doi.org/10.1086/522774)

Peng, C. Y., Impey, C. D., Ho, L. C., Barton, E. J., & Rix, H.-W. 2006, ApJ, 640, 114, doi: [10.1086/499930](https://doi.org/10.1086/499930)

Phinney, E. S. 2001, A Practical Theorem on Gravitational Wave Backgrounds, arXiv, doi: [10.48550/ARXIV.ASTRO-PH/0108028](https://doi.org/10.48550/ARXIV.ASTRO-PH/0108028)

- Reardon, D. J., Zic, A., Shannon, R. M., et al. 2023, *ApJL*, 951, L6, doi: [10.3847/2041-8213/acdd02](https://doi.org/10.3847/2041-8213/acdd02)
- Rodriguez-Gomez, V., Genel, S., Vogelsberger, M., et al. 2015, *MNRAS*, 449, 49, doi: [10.1093/mnras/stv264](https://doi.org/10.1093/mnras/stv264)
- Sah, M. R., & Mukherjee, S. 2024, arXiv e-prints, arXiv:2407.11669, doi: [10.48550/arXiv.2407.11669](https://doi.org/10.48550/arXiv.2407.11669)
- Sah, M. R., Mukherjee, S., Saeedzadeh, V., et al. 2024, *MNRAS*, 533, 1568, doi: [10.1093/mnras/stae1930](https://doi.org/10.1093/mnras/stae1930)
- Sato-Polito, G., Zaldarriaga, M., & Quataert, E. 2024, *PhRvD*, 110, 063020, doi: [10.1103/PhysRevD.110.063020](https://doi.org/10.1103/PhysRevD.110.063020)
- Schechter, P. 1976, *ApJ*, 203, 297, doi: [10.1086/154079](https://doi.org/10.1086/154079)
- Sesana, A., Haardt, F., Madau, P., & Volonteri, M. 2004, *ApJ*, 611, 623, doi: [10.1086/422185](https://doi.org/10.1086/422185)
- Shankar, F., Bernardi, M., Sheth, R. K., et al. 2016, *MNRAS*, 460, 3119, doi: [10.1093/mnras/stw678](https://doi.org/10.1093/mnras/stw678)
- Shankar, F., Bernardi, M., Richardson, K., et al. 2019, *MNRAS*, 485, 1278, doi: [10.1093/mnras/stz376](https://doi.org/10.1093/mnras/stz376)
- Shen, X., Hopkins, P. F., Faucher-Giguère, C.-A., et al. 2020, *MNRAS*, 495, 3252, doi: [10.1093/mnras/staa1381](https://doi.org/10.1093/mnras/staa1381)
- Shimizu, T., Oogi, T., Okamoto, T., Nagashima, M., & Enoki, M. 2024, *MNRAS*, 531, 851, doi: [10.1093/mnras/stae1226](https://doi.org/10.1093/mnras/stae1226)
- Simon, J. 2023, *ApJL*, 949, L24, doi: [10.3847/2041-8213/acd18e](https://doi.org/10.3847/2041-8213/acd18e)
- Skelton, R. E., Whitaker, K. E., Momcheva, I. G., et al. 2014, *ApJS*, 214, 24, doi: [10.1088/0067-0049/214/2/24](https://doi.org/10.1088/0067-0049/214/2/24)
- Sun, Y., Lyu, J., Rieke, G. H., et al. 2025, *ApJ*, 978, 98, doi: [10.3847/1538-4357/ad973b](https://doi.org/10.3847/1538-4357/ad973b)
- Tacchella, S., Diemer, B., Hernquist, L., et al. 2019, *MNRAS*, 487, 5416, doi: [10.1093/mnras/stz1657](https://doi.org/10.1093/mnras/stz1657)
- Tanaka, T. S., Silverman, J. D., Ding, X., et al. 2025, *ApJ*, 979, 215, doi: [10.3847/1538-4357/ad9d0a](https://doi.org/10.3847/1538-4357/ad9d0a)
- Terrazas, B. A., Aird, J., & Coil, A. L. 2024, arXiv e-prints, arXiv:2411.08838, doi: [10.48550/arXiv.2411.08838](https://doi.org/10.48550/arXiv.2411.08838)
- Tomczak, A. R., Quadri, R. F., Tran, K.-V. H., et al. 2014, *ApJ*, 783, 85, doi: [10.1088/0004-637X/783/2/85](https://doi.org/10.1088/0004-637X/783/2/85)
- Trakhtenbrot, B., & Netzer, H. 2010, *MNRAS*, 406, L35, doi: [10.1111/j.1745-3933.2010.00876.x](https://doi.org/10.1111/j.1745-3933.2010.00876.x)
- van den Bosch, R. C. E. 2016, *ApJ*, 831, 134, doi: [10.3847/0004-637X/831/2/134](https://doi.org/10.3847/0004-637X/831/2/134)
- van der Wel, A., Franx, M., van Dokkum, P. G., et al. 2014, *ApJ*, 788, 28, doi: [10.1088/0004-637X/788/1/28](https://doi.org/10.1088/0004-637X/788/1/28)
- Virtanen, P., Gommers, R., Oliphant, T. E., et al. 2020, *Nature Methods*, 17, 261, doi: [10.1038/s41592-019-0686-2](https://doi.org/10.1038/s41592-019-0686-2)
- Volonteri, M. 2012, *Science*, 337, 544, doi: [10.1126/science.1220843](https://doi.org/10.1126/science.1220843)
- Wagenmakers, E.-J., Lodewyckx, T., Kuriyal, H., & Grasman, R. 2010, *Cognitive Psychology*, 60, 158, doi: <https://doi.org/10.1016/j.cogpsych.2009.12.001>
- Wright, A. H., Driver, S. P., & Robotham, A. S. G. 2018, *MNRAS*, 480, 3491, doi: [10.1093/mnras/sty2136](https://doi.org/10.1093/mnras/sty2136)
- Wyithe, J. S. B., & Loeb, A. 2003, *ApJ*, 595, 614, doi: [10.1086/377475](https://doi.org/10.1086/377475)
- Xu, H., Chen, S., Guo, Y., et al. 2023, *Research in Astronomy and Astrophysics*, 23, 075024, doi: [10.1088/1674-4527/acdfa5](https://doi.org/10.1088/1674-4527/acdfa5)
- Yue, M., Eilers, A.-C., Simcoe, R. A., et al. 2024, *ApJ*, 966, 176, doi: [10.3847/1538-4357/ad3914](https://doi.org/10.3847/1538-4357/ad3914)
- Zhang, Y., Ouchi, M., Gebhardt, K., et al. 2023, *ApJ*, 948, 103, doi: [10.3847/1538-4357/acc2c2](https://doi.org/10.3847/1538-4357/acc2c2)
- Zhuang, M.-Y., & Ho, L. C. 2023, *Nature Astronomy*, doi: [10.1038/s41550-023-02051-4](https://doi.org/10.1038/s41550-023-02051-4)